GROWTH AND CHARACTERIZATION OF ALUMINUM DOPED TRANSPARENT AND CONDUCTIVE ZINC OXIDE THIN FILMS

A Thesis submitted to
The Graduate School of Engineering and Science of
İzmir Institute of Technology
in Partial Fulfillment of the Requirements for the Degree of

MASTER OF SCIENCE

in Physics

by

Derya ATAÇ

April 2010
İZMİR

We approve the thesis of **Derya ATAÇ**

_____

Assist. Prof. Dr. Yusuf SELAMET
Supervisor

_____

Assist. Prof. Dr. Enver TARHAN
Committee Member

_____

Assist. Prof. Dr. Ömer MERMER
Committee Member

29 April 2010

_____

Prof. Dr. Nejat BULUT
Head of the Department of Physics

_____

Assoc. Prof. Dr. Talat YALÇIN
Dean of the Graduate School of
Engineering and Sciences

ACKNOWLEDGEMENTS

I want to thank to İzmir Institute of Technology Department of Physics for giving me the chance to be a member of scientific study and supporting me as a research assistant during my master.

There are so many people I want to thank for helping me complete my study.

Firstly, I would like to express my respect and gratitude my supervisors Assist. Prof. Dr. Süleyman Tarı and Assist. Prof. Dr. Yusuf Selamet. I would like to thank Dr. Süleyman Tarı for his trust and accepting me as his student in the first place. He always made feel that he had confidence in me and he always had an open door for me. His patience, guidance, ingenious remarks and comments helped me finish this study.

I can not thank enough to Dr. Yusuf Selamet for being there for me during difficult times of my study. He answered all my questions in detail with patience and he never hesitated to spend his valuable time to help me. I definitely would not complete this study without his continuous support, guidance, patience and help. I will always remember and be inspired by both of my supervisors' hard work and good hearts.

I would like to thank to the members of my defense committee Assist. Prof. Dr. Enver Tarhan, Assist. Prof. Dr. Ömer Mermer, Assist. Prof. Dr. Ekrem Özdemir and Prof. Dr. Orhan Öztürk for their valuable comments. I thank Prof. Dr. Serdar Özçelik for optical characterization of my samples and his comments. I want to thank to Dr. Salih Okur and Dr. Orhan Öztürk for giving me the opportunity to use AFM and XRD instruments whenever I needed. I especially want to thank Serdal Okur, Serkan Büyükköse, Nesli T. Yağmurcukardeş and Hasan Aydın for spending their invaluable time for XRD and AFM measurements (for their warm friendship). My thanks go to IYTE Material Research Center staff for SEM images.

I want to thank each one of my friends from İYTE for things we shared and enjoyable time we spent. Their warm friendship provided motivation and made it an enjoyable thing to stay at school to work at night. Going to breakfast (beginning the day with chatting), lunch and dinners (accompanied with enjoyable conversation and followed by warm tea) are things I will remember with joy for the rest of my life.

I want to express my thanks beginning with my graduated lab mates Hüseyin Tokuç and Hüseyin Serhat Alagöz for the things they had thought me. Their friendship made our lab an enjoyable place to work.

I feel privileged to have a friend like Barış Pekerten. I am grateful to him for his support, help, beautiful friendship and good heart. I feel very lucky to have Serkan Büyükköse by my side since my first day in IYTE. I thank him for his friendship, love, sharing and being there like a stone whenever I needed. I thank both Barış and Serkan for being a role model to me by showing how to work hard and get joy from work. I thank Tuna Demircik for chats and laughs we had during the time we spent.

I especially want to thank Hale Sert, my long lasting friend since the first week of our undergraduate school, deserves special thanks. She had been by my side in good days and bad days listening, advising, easing my troubles and cheering me up. I feel more than lucky to have her by my side all these years.

I am thankful to have met my beautiful friend Atike İnce with whom we had heart to heart talks and shared bitter sweet days together . Besides her good heart and warm friendship, I thank her for convincing me to begin tango. I want to be able to work with Hale and Atike again in the future with all my heart.

My special thanks go to my undergraduate friends from Dokuz Eylül University; Nihan Özkan, Nevin Soylu (for opening their home to us 7/24, for delicious breakfasts, dinners and giving us the opportunity to have so much fun), Feyzan Özgün Ersoy, Duygu Dörtlemez and Filiz Aksoy. I learned a lot from each and I feel very luck to have friends like them as I was growing up. I thank them for every day we spend since the day we first met.

I want to mention my dear friends Çağrı Mazlum and Ece Başokur, for sharing beautiful memories and being in my life since middle school. I want to thank Seçkin Türkcan for his care, support and things we shared for all these years since high school.

I feel privileged to have met and study with the valuable scientists of IYTE. I want thank them for teaching and sharing their experiences with us. I hope I can be as lucky to work with them again in coming days.

Last, but most importantly, I want to thank my family stating with my precious mother Suten Ataç and father Mehmet Ataç. I am grateful to them for their endless support, patience, generosity, love and faith in me. I would not have accomplished anything without them by my side. I thank to my dear brother Denizhan Ataç, his lovely wife Filiz Ataç and my sweet and brilliant niece Derin Ataç for the joy and happiness they brought into my life.

I apologize to those whom I unwillingly forgot to mention. I wish all my loved ones to have a happy and successful life.

ABSTRACT

GROWTH AND CHARACTERIZATION OF ALUMINUM DOPED TRANSPARENT AND CONDUCTIVE ZINC OXIDE THIN FILMS

This thesis focuses on fabrication, characterization and understanding physical properties of transparent and conductive Al doped zinc oxide (ZnO) thin films. Films were deposited by magnetron sputtering technique, using separate ZnO and Al targets. SiO_2 and glass (microscope slides) were used as substrates. Growths were performed at room temperature in Ar environment at a constant pressure of 3 mTorr. Films were characterized by atomic force microscope, x-ray diffractometer, scanning electron microscope, UV-vis spectroscophotometer and four point probe electrical measurements. Using transmission data, band gaps of the films and using four point probe measurements, resistivities of films were calculated. Firstly properties of pure ZnO films were studied. They were found to be highly transparent; however their resistivity was very high that we could not measure with our instrument. Therefore, ZnO films were uniformly doped with Al. It was seen that decreasing Al content was improving electrical and optical properties. Al concentration of the films was decreased firstly by decreasing deposition power of Al. After that, content was further decreased by depositing stacks of doped and undoped layers (modulation doping). Following that, modulation doped films were deposited with applying RF bias power to substrates. All films were annealed at 300^oC for 1 hour in vacuum. The lowest resistivity obtained in this study was $1.68x10^{-3}$ Ωcm. Transmittance and band gap of the corresponding film were 80% and 4.1 eV respectively. The film was fabricated by modulation doping accompanied with substrate bias of 10 W, followed by annealing at 300^oC in vacuum.

ÖZET

ALUMİNYUM İLE SAFSIZLAŞTIRILMIŞ ÇİNKO OKSİT SAYDAM VE İLETKEN İNCE FİLMLERİN ÜRETİLMESİ VE KARAKTERİZASYONU

Bu tez, Al ile safsızlaştırılmış iletken ve saydam çinko oksit (ZnO) ince filmlerin üretimi, karakterizasyonu ve fiziksel özelliklerinin anlaşılması üzerinde odaklanmıştır. Filmler, ZnO ve Al hedefler kullanılarak manyetik saçtırma yöntemiyle büyütülmüştür. Alt taşı olarak SiO_2 ve cam (mikroskop slaydı) kullanılmıştır. Büyütme işlemleri oda sıcaklığında, Ar atmosferinde 3 mTorr sabit basınç altında gerçekleştirilmiştir. Filmler atomik güç mikroskobu, x-ışını kırınımı cihazı, taramalı elektron mikroskobu, UV spektrofotometresi ve dört nokta probu elektriksel ölçüm teknikleriyle karakterize edilmiştir. Filmlerim geçirgenlik verilerinden yararlanılarak optik band aralıkları, dört nokta probu ölçümlerinden yararlanılarak özdirenç değerleri hesaplanmıştır. Çalışmada, öncelikle saf ZnO filmlerin özellikleri incelenmiştir. Saf ZnO filmlerin oldukça saydam, ancak dirençlerinin sistemimizde ölçemeyeceğimiz kadar yüksek olduğu görülmüştür. Ardından filmler Al ile katkılanmıştır. Al konsantrasyonun azalmasıyla filmlerin elektriksel ve optik özelliklerinin daha iyiye gittiği gözlenmiştir. Filmlerin Al katkı oranları ilk önce Al saçtırma gücü düşürülerek azaltılmıştır. Bunu takiben, filmler katkılı ve katkısız katmanların üst üste büyütülmesiyle hazırlanmıştır (düzenlemeli safsızlaştırma metodu). Bundan sonra, filmler bu metoda ek olarak alt taşlarına besleme gücü uygulayarak büyütülmüştür. Bütün filmler ayrıca 300^oC de bir saat boyunca vakumda tavlanmıştır. Bu çalışmada elde edilen en düşük özdirençli Al katkılı ZnO film $1.68x10^{-3}$ Ωcm özdirencine, %80 geçirgenliğe ve 4.1 eV band aralığına sahiptir. Söz konusu film düzenlemeli safsızlaştırma yöntemi ile alt taşına 10 W besleme gücü uygulanarak büyütülmesi ve ardından 300^oC de vakum ortamında tavlanmasıyla elde edilmiştir.

To my Family

TABLE OF CONTENTS

LIST OF FIGURES x

LIST OF TABLES xiii

CHAPTER 1. INTRODUCTION 1

1.1. Transparent Conducting Oxides 2

1.2. Applications of Transparent Conducting Oxides 5

CHAPTER 2. ZINC OXIDE (ZnO) 7

2.1. Properties of ZnO 8

2.1.1. Crystal Structure of ZnO 8

2.1.2. Electrical Properties of ZnO 10

2.1.2.1. Intrinsic Dopants 11

2.1.2.2. Extrinsic Dopants 12

2.1.3. Optical Properties of ZnO 12

2.1.4. Scattering Processes 14

2.2. Advantages and Disadvantages of ZnO 15

2.3. Applications of ZnO 17

2.4. Deposition Methods of ZnO 18

CHAPTER 3. EXPERIMENTAL DETAILS 20

3.1. Sample Preparation 20

3.1.1. Sample Cleaning Process 20

3.1.2. Thin Film Deposition 21

3.1.3. Magnetron Sputtering Technique 21

3.1.3.1. DC Magnetron Sputtering 22

3.1.3.2. RF Magnetron Sputtering 23

3.1.3.3. Reactive Magnetron Sputtering 23

3.1.4. Growth Procedure 25

CHAPTER 4. RESULTS AND DISCUSSION 29
4.1. Properties of Pure ZnO 29
4.1.1. Characterization of Pure ZnO 30
4.1.1.1. Resistivity of Pure ZnO 30
4.1.1.2. Thickness and Roughness of Pure ZnO 30
4.1.1.3. XRD Results of Pure ZnO 32
4.1.1.4. SEM Results of Pure ZnO 35
4.1.1.5. Transmission Results of Pure ZnO 36
4.1.1.6. Band Gap of ZnO Films of Pure ZnO 38
4.2. Effect of Al Content 41
4.2.1. XRD Results 42
4.2.2. SEM Results 43
4.2.3. Resistivity Results 44
4.2.4. Transmission Results 46
4.3. Effect of Modulation Doping 48
4.3.1. XRD Results 50
4.3.2. SEM Results 52
4.3.3. Resistivity 54
4.3.4. Transmission 55
4.4. Effect of Substrate Bias 59
4.4.1. XRD Results 59
4.4.2. SEM Results 61
4.4.3. Resistivity 61
4.4.4. Transmission 62
4.5. Annealing Effect 65
4.5.1. XRD Results for Annealed Samples 66
4.5.2. SEM Results 67
4.5.3. Transmission Results 68
4.5.4. Resistivity 69
4.6. Summary 70

CHAPTER 5. CONCLUSIONS 72

REFERENCES 76

LIST OF FIGURES

Figure **Page**

Figure 1.1. Reported resistivity of impurity-doped binary compound TCO films, 1972 present: impurity-doped SnO2 (triangles), In_2O_3 (squares) and ZnO (dots). 5

Figure 2.1. The hexagonal wurtzite structure of ZnO. O atoms are shown as large white spheres, Zn atoms as smaller black spheres (Source: Coleman 2006). 8

Figure 2.2. Two views of the crystal structure of zinc oxide (ZnO). Left : Perspective view perpendicular to the c-axis. Right : View along the c-axis on the zinc terminated (0001) plane, the bottom plane is oxygen terminated $(000\bar{1})$. (Source: Ellmer, et al. 2008). 9

Figure 2.3. (a) The rock salt and (b) zincblende phases of ZnO. O atoms are shown as white spheres, Zn atoms as black spheres. One unit cell is illustrated (Source: Coleman 2006). 10

Figure 2.4. A simplified band gap description of TCOs: (a) without impurities, (b) band gap widening (c) band gap narrowing (Source: Bashar 1998).....14

Figure 3.1. Illustration of magnetron sputtering process. 22

Figure 3.2. ATC Orion 5 UHV Magnetron Sputtering System 25

Figure 3.3. Codeposition of ZnO and Al. 25

Figure 3.4. Illustration of carrier transport in uniformly and modulation doped structures. 27

Figure 4.1. Thickness vs deposition time plot for pure ZnO on glass substrates. 31

Figure 4.2.Roughness values for ZnO films on glass and SiO_2/Si substrates.... 32

Figure 4.3. XRD results for pure ZnO films of various thicknesses grown on glass substrates. 33

Figure 4.4. Grain size of ZnO (002) peaks of films with various thicknesses. Inset shows FWHM vs films thickness. 34

Figure 4.5. Lattice strain of ZnO (002) peaks of films with various thicknesses. 35

Figure 4.6. SEM image of 20 nm ZnO. 36

Figure 4.7. Cross sectional SEM image of ZnO. 36

Figure 4.8. Transmission data of pure ZnO films of various thicknesses on glass substrates. Inset shows average transmission of the films between wavelengths of 400-800nm. 37
Figure 4.9. Extrapolation for defining band gap of pure ZnO films. 40
Figure 4.10. A Closer look into Figure 4.9 between energies 2.5 and 3.5 eV. 40
Figure 4.11. Absorption energies of pure ZnO with various thicknesses. 41
Figure 4.12. XRD patterns of Al doped ZnO films with various Al contents. 43
Figure 4.13. SEM images of Al dopped films with Al deposition power of (a), (b) 20 W and (c), (d) 5 W. (a) and (b) have 500nm scales while (c) and (d) have 200 nm scales 44
Figure 4.14. Resistivity values of Al doped ZnO films with various Al contents. 45
Figure 4.15. Transmission spectra of Al doped ZnO films with various Al contents. ... 46
Figure 4.16. Average transmission between 400-800 nm of Al doped ZnO films. 47
Figure 4.17. Band gap values of Al doped ZnO films. 48
Figure 4.19. XRD pattern for films with varying transport layer thicknesses. 51
Figure 4.20. (a) Grain sizes of ZnO (002) peaks of modulation dopped films. 52
Figure 4.21. SEM images of modulation doped films. 53
Figure 4.22. SEM images of (a) uniformly doped and (b) modulation doped (pure ZnO layer thickness: 1,5 nm). 53
Figure 4.23. Resistivity of films with various transport layer (ZnO) thickness. 54
Figure 4.24. Transmission spectra of modulation doped films. 56
Figure 4.25. Average transmission between wavelengths 400-800 nm of modulation doped films 56
Figure 4.26. Square of absorption coefficient vs photon energy plot for band gap energy calculation of modulation doped films 58
Figure 4.27. Band gap energy of modulation doped films. 58
Figure 4.28. XRD patterns of biased samples 60
Figure 4.29. SEM images of films deposited (a) without substrate bias and (b)with 10 W substrate bias. 61
Figure 4.30. Resistivity vs applied bias power. 62
Figure 4.31. Transmission spectra of biased films. 63
Figure 4.32. Average transmission of biased samples between 400-800 nm. 64
Figure 4.33. Extrapolation for defininition of band gaps of biased samples. 64
Figure 4.34. Band gaps of biased samples. 65

Figure 4.35. Annealed and as grown XRD spectrums of lowest resistivity samples of each set (a) pure ZnO, (b) uniformly doped; (c) modulation doped, and (d) biased samples. 66
Figure 4.36. Comparison of (a,b,c) as grown and (d,e,f) annealed uniformly doped ZnO films. (lowest resistivity films of each set.) (a,d) uniformly doped (b,e) modulation doped, and (c,f) biased samples.....67
Figure 4.37. Average transmission and band gap values of annealed and non annealed samples (modulation doped and biased samples). 69
Figure 4.38. Resistivites of annealed and non annealed (a) modulation doped and (b) biased samples.....70
Figure 4.39. Resistivity and transmission values of lowest resistivity films of uniformly doped, modulation doped and substrate biased films. 71

LIST OF TABLES

Table **Page**

Table 1.1. Electrical properties of common transparent conducting oxides (TCOs).....3

Table 4.1. Deposition parameters of pure ZnO samples..... 30

Table 4.2. Growth parameters, thickness, roughness and calculated Al content of Al doped ZnO films. 42

Table 4.3. Pure ZnO layer (transport layer) thickness, total thickness and corresponding Al content of films. 50

Table 4.4. Deposition parameters for growth of biased samples..... 59

CHAPTER 1

INTRODUCTION

It is known that transparent materials are usually insulators and metals are usually not transparent. Transparent conducting oxides (TCOs) are special semiconductors that have advantage of transparency to visible light and conductivity close to that of metals. These materials are employed in transparent electronics. Some applications of TCOs include invisible circuits for security applications, flat and flexible panel displays, touch screens, transparent monitors. TCOs are also used as front contacts for solar cell devices, where light enters the device.

Most used TCO on the market is In doped Tin Oxide (ITO) owing to its low resistivity ($1x10^{-4}$ Ωcm) and high transparency (>80%). However, In is a rare element which increases its cost. It is also projected that it will fail to cover rising demand. Indium is toxic. Owing to these facts, alternative elements for ITO are being searched. We chose to investigate Al doped ZnO (AZO) due to its resistivity and transparency comparable to ITOs.

In this study, we focused on producing Al doped ZnO films with low resistivity and high transparency in visible range. We tried to fabricate conducting Al doped ZnO films with magnetron sputtering technique. We studied structural, optical and electrical characterizations on these films.

Although AZO can be deposited with other techniques like PLD (Singh and Mehra 2001), MOCVD (Fragala, et al. 2009), we chose magnetron sputtering because amongst these techniques, magnetron sputtering has advantages such as availability to produce highly transparent and conducting films, easy fabrication and most importantly applicability to large samples, enabling industrial fabrication. Reports on magnetron sputtered AZO films with resistivities of $1.9x\ 10^{-4}$ and $2.7x\ 10^{-4}$ were published by Minami, et al. (1984).

We investigated Al content in the structures because carrier concentration affects optical and electrical properties of ZnO films significantly and defines whether these films can be used in industrial applications.

Sputtering of AZO films from sintered AZO ceramic targets with various Al contents are widely studied in the literature (Jeong and Park 2002, Hao, et al. 2006). We deposited AZO from separate ZnO and Al targets, because metallic (Al) targets are cheaper than ceramic (AZO) targets. Also individual Al target enables to change Al content easily; otherwise, new ceramic targets for several carrier concentrations would be needed, which would increase the cost of the investigation.

We decreased the Al content of the films with 3 different processes. In the first one, we decreased the deposition power of Al form 20 W to 2.5 W. The lowest resistivity was achieved with 5 W. Therefore, we defined deposition power of Al as 5 W for the rest of the study. In the second process, in order to decrease the total Al content, we deposited periodic stacks of doped layers and pure ZnO layers. In the structure, doped layers acted as carrier supply, while undoped layers acted as transport layer for carriers supplied from doping layer. We fixed the thicknesses of doped layers at about 1 nm, whereas thicknesses of pure ZnO layers were varied between ~0.5 nm and ~3 nm. We observed that resistivity of the films decreased and transmission increased. We illustrated this effect as elimination of ionized impurity scattering due to separation of carriers from ionized impurities. In the third process, we applied RF bias power to substrates, aiming to decrease the growth rate of Al and ZnO. This process also showed that resistivity decreased and transmission increased. Apart from these 3 processes, we applied post deposition annealing to all samples. We annealed the samples at 300^{o}C for 1 hour in vacuum environment. We saw that resistivities of the samples were dropping to half, while transmittance of the samples remained almost the same.

This thesis consists of 5 chapters. In the first chapter, properties and applications of TCOs are introduced. In the second chapter, detailed information about ZnO is given. The third chapter contains experimental details and result are given and discussed in the fourth chapter. In the last chapter, conclusions about the work are presented.

1.1. Transparent Conducting Oxides

Transparent conducting oxides (TCOs) are interesting semiconductors that possesses two physical properties: high optical transparency in visible range and high electrical conductivity (Wager, et al. 2008). In order to exhibit those properties, TCOs should have large band gaps of about 3 eV, their resistivity must be on the order of

about 10^{-4} Ωcm and they should have a high enough concentration of electrical carriers, i.e., an electron or hole concentration > ~10^{19} cm^{-3} with a sufficiently large mobility, > ~1 cm^2 $V^{-1}s^{-1}$ (Wager, et al. 2008).

Why large band gaps are required for high optical transmission in TCOs can be expressed in terms of electron transition. When light enters the TCO, the photons with energies higher than band gap of the TCO are absorbed, which means that those photons can not pass through the TCO. However, the photons with lower energies than the band gap can not be absorbed and they pass through the TCO, which makes the TCO transparent for the wavelengths corresponding to those lower photon energies. Therefore, high optical transmission requires large band gaps (>3 eV).

In order to obtain lower resistivities, several TCO thin films consisting of binary, ternary and multicomponent compounds are developed. Binary compounds are more advantageous because controlling their chemical composition during deposition is easier (Minami 2005).

The most common binary compound TCOs are indium oxide (In_2O_3), tin oxide (SnO_2), cadmium oxide (CdO) and zinc oxide (ZnO). Electrical properties of these materials are given in Table 1.

Table 1.1. Electrical properties of common transparent conducting oxides (TCOs) Resistivities reported are for best-case n-type polycrystalline films (Source: Wager, et al. 2008).

Material	**Band Gap (eV)**	**Resistivity (Ωcm)**
In_2O_3	3.75	$1x10^{-4}$
ZnO	3.35	$1.25x10^{-4}$
SnO_2	3.60	$2x10^{-4}$
CdO	2.16	$3x10^{-2}$

All of the well-known and commercially relevant TCOs are n-type. p-type TCOs are a relatively new phenomenon and their conductivity performance is quite poor compared to that of n-type TCOs (Wager, et al. 2008).

With metal oxides, it is also possible to deposit highly transparent and conducting films without intentional impurity doping (Dawar and Joshi 1984,

Hartnagel, et al. 1995). The films are n type degenerated semiconductors with free electron concentrations of 10^{20} cm^{-3} provided by native donors such as oxygen vacancies and/or interstitial metal atoms (Minami 2005). However, compounds without impurity doping are observed to be unusable in practical use because when used at high temperatures they were found to be unstable (Minami, et al. 1984).

ITO, with low resistivities and high optical transparency is the most widely used TCO films on the market. ITO thin films deposited by magnetron sputtering with resistivities on the order of $1x10^{-4}$ Ωcm are commercially available today. Also resistivities as low as $7.2x10^{-5}$ Ωcm are reported for ITO films deposited by pulsed laser deposition (Suzuki, et al. 2001). However, scarcity of In rises the prize of the material and toxic effect of the material leads to health concerns. Therefore, new materials with resistivities as low as ITOs to replace ITO are being searched. One promising candidate is Al doped ZnO owing to its abundance, low cost, nontoxicity and low resistivity (comparable to the resistivity of ITO). Suzuki, et al. have prepared a report on impurity-doped ZnO thin films with the level of resistivity of ITOs which is $5x10^{-5}$ Ωcm (2001). Also reports on magnetron sputtered Al doped ZnO films with resistivities of $1.9x\ 10^{-4}$ and $2.7x\ 10^{-4}$ were reported by Minami, et al. (1984). It is also noteworthy that the obtained minimum resistivities of impurity-doped ZnO films is still decreasing, whereas those of impurity-doped SnO_2 and In_2O_3 films have essentially remained unchanged for more than the past twenty years as can be seen in Figure 1.1 (Minami 2005).

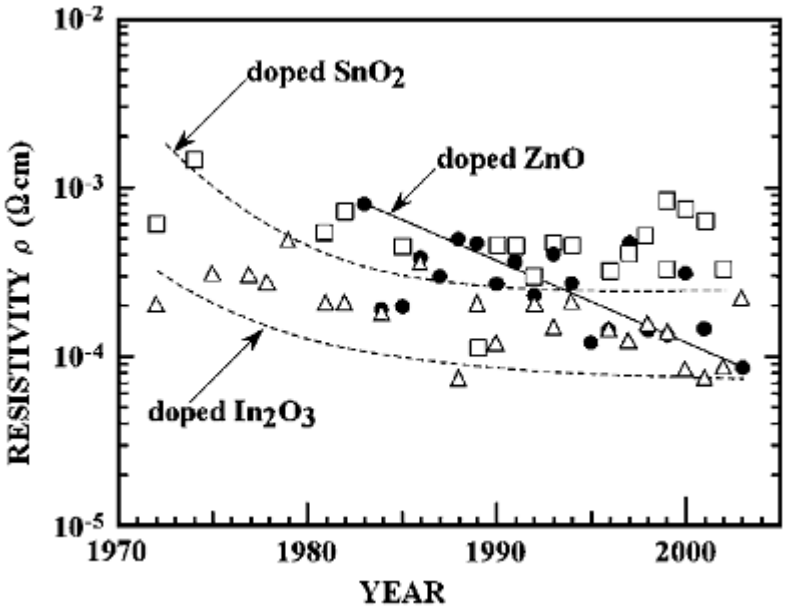

Figure 1.1. Reported resistivity of impurity-doped binary compound TCO films, 1972 present: impurity-doped SnO_2 (triangles), In_2O_3 (squares) and ZnO (dots) (Source: Minami 2005).

1.2. Applications of Transparent Conducting Oxides

Transparent conducting oxide films are used in a variety of applications. Some applications of TCOs can be listed as follows:

TCOs find application in *solar cells*. The front surface of solar cells require a transparent and conducting layer so that light falling on the cell would pass the most of the light to the absorber layers and a full circuit may e formed for the generated photocurrent to be completed. ITO and Al doped ZnO are the most preferable materials for this application (Gordon 2000).

Low emissivity windows for energy saving for both hot and cold climates may be produced with TCOs. This is achieved by taking the plasma frequency of the materials into consideration. At frequencies higher than the plasma frequency, the electrons can not respond, therefore the material acts like a transparent dielectric for incident radiation. On the other hand, at frequencies below the plasma frequency, the TCO reflects and absorbs the incident radiation. For example, in hot climates, if TCOs with short plasma wavelengths are used, near-infrared portion of sunlight will reflect out of the building and the building would be protected from extra heating. In cold climates if

TCOs with long plasma lengths are used, most of solar spectrum would transmit into the building and turn into heat by reflections inside the building.

Defrosting windows in airplanes was the first applications of ZnO during World War II and kept as a secret until the end of the war. Today, defrosting windows are used in freezers of supermarkets. Electric current is passed through the display windows of the freezers in order to prevent the moisture in air condense on the window.

TCOs are employed in *oven windows* in order to improve safety by lowering the surface temperature to harmless levels. This application can also be seen in self cleaning ovens that reach very high temperatures. Some laboratory ovens are also made of TCO coated glass which also serves as resistor for heating the oven.

TCOs are used in *flat panel displays (FPD)* too. For this application, the TCO should have good conductivity and easy etchability. ITO is preferable for this application, however ZnO is a strong candidate to replace ITO owing to its lower cost and easier etchability.

Touch panel controls which can be seen on appliances, elevator controls, ATM screens are built from etched TCO on glass. They sense the presence of a finger either by direct contact or capacively through the glass.

TCOs may also be hired as a part of invisible *security circuits* for windows or glass over valuable works of art. Also some protection from UV light may be provided as well.

CHAPTER 2

ZINC OXIDE (ZnO)

ZnO is a II-VI semiconductor that consists of Zinc ($_{30}$Zn) and Oxygen ($_{8}$O), belonging to 6th and 2nd group of periodic table.

Although ZnO was being investigated in 1912, systematic research on ZnO as a compound semiconductor started with the invention of transistor. In 1960, the good piezoelectric properties of ZnO were discovered, which was followed by the first electronic application of ZnO as a thin layer for surface acoustic wave devices. Today, ZnO is a material of interest owing to its prospective use as a wide band gap semiconductor for light emitting devices and for transparent or high temperature electronics (Ellmer, et al. 2008).

ZnO is a wide band gap semiconductor, with a band gap of 3.3 eV. Its wide band gap makes pure ZnO colorless and clear in the visible region. Therefore, it can be used in transparent electronics. In addition to good transparency, it also has good electron mobility.

ZnO has some other favorable properties like low power threshold for optical pumping, radiation hardness, biocompatibility and broad chemistry leading to many opportunities for wet chemical etching (which is necessary for device fabrication as it increases the properties of the device) (Coleman and Jagadish 2006).

In order to use ZnO for transparent conducing oxide applications, it is sufficient to produce ZnO with low resistivity and high transparency. This can be achieved by introducing either intrinsic or extrinsic dopants. However intrinsic doping was observed to be result in insufficient conductivity, therefore extrinsic doping is preferred.

ZnO is usually prepared as n type semiconductor. p type ZnO is harder to prepare because solubility of p type dopants is less compared to n type dopants.

2.1. Properties of ZnO

ZnO is a widely studied semiconductor owing to its crystal structure, mechanical, electrical and optical properties. Crystal structure, mechanical, electrical and optical properties of ZnO is presented in the following parts of this chapter.

2.1.1. Crystal Structure of ZnO

At ambient temperature and pressure, ZnO preferentially crystallizes in wurtzite structure as can be seen in Figure 2.1. This is a hexagonal lattice and is characterized by two interconnected sublattices of Zn^{+2} and O^{-2}, such that each Zn ion is surrounded by a tetrahedral of O ions and vice versa. This tetrahedral coordination results in polar symmetry along the hexagonal axis. This polarity leads to a number of the properties of ZnO, including piezoelectricity and spontaneous polarization, and is also a key factor in crystal growth, etching and defect generation (Coleman 2006).

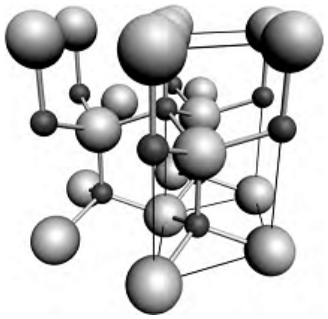

Figure 2.1. The hexagonal wurtzite structure of ZnO. O atoms are shown as large white spheres, Zn atoms as smaller black spheres (Source: Coleman 2006).

The four most common face terminations of wurtzite ZnO are the polar Zn terminated (0001) and O terminated $(000\bar{1})$ faces (c-axis oriented), and the non-polar $(11\bar{2}0)$ (a-axis) and $(10\bar{1}0)$ faces which both contain an equal number of Zn and O atoms. The polar faces, shown in Figure 2.2, are known to posses different chemical and physical properties, and the O-terminated face possesses a slightly different electronic structure to the other three faces. Additionally, the polar surfaces and the (1010) surface

are found to be stable; however the $(11\bar{2}0)$ face is less stable and generally has a higher level of surface roughness than its counterparts (Coleman 2006). The lattice parameters of the hexagonal unit cell are a=3.2495Å and c=5.2069Å, and the density is 5.605 gcm^{-3} (Lide, et al. 1992).

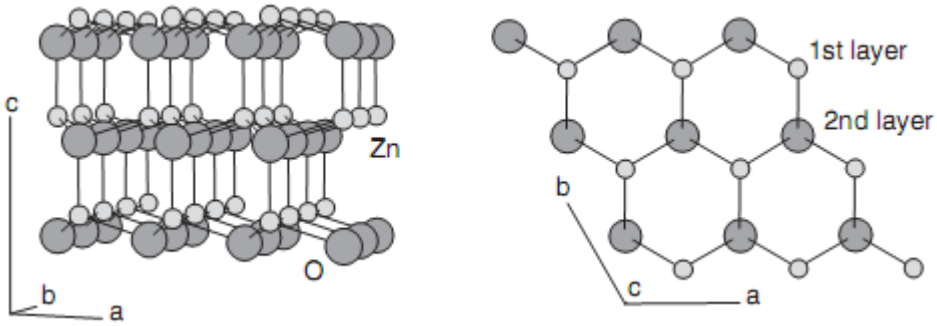

Figure 2.2. Two views of the crystal structure of zinc oxide (ZnO). Left : Perspective view perpendicular to the c-axis. Right : View along the c-axis on the zinc terminated (0001) plane, the bottom plane is oxygen terminated $(000\bar{1})$. (Source: Ellmer, et al. 2008).

Aside from causing the inherent polarity in the ZnO crystal, the tetrahedral coordination of this compound is also a common indicator of sp^3 covalent bonding. However, the Zn–O bond also possesses very strong ionic character, and thus ZnO lies on the borderline between being classed as a covalent and ionic compound. Zn face possesses more covalent character, arising from the Zn 4s - O 2p states, whilst the O face is more ionic (Coleman 2006).

Additional to the wurtzite phase, ZnO is also known to crystallize in the cubic zincblende and rocksalt (NaCl) structures, which are illustrated in Figure 2.3. Zincblende ZnO is stable when grown on cubic strucures (Chopra, et al. 1983), whereas rocksalt structure is a high pressure metastable phase and can not be epitaxially stabilized (Bates, et al. 1962).

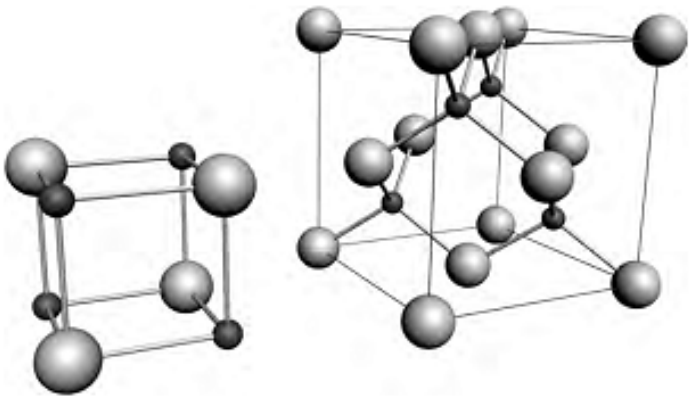

Figure 2.3. (a) The rock salt and (b) zincblende phases of ZnO. O atoms are shown as white spheres, Zn atoms as black spheres. One unit cell is illustrated (Source: Coleman 2006).

ZnO is highly susceptible to humidity and temperature. Reason for susceptibility is the crystal structure of ZnO. Hydrogen and oxygen in water can easily diffuse in zinc oxide's crystal structure. The hydrogen and oxygen react with film elements, disrupting the normal balance between the Zn and oxygen due to an oxidation-reduction reaction to inhibit conductive performance (Suzuki 2009).

2.1.2. Electrical Properties of ZnO

ZnO mostly show n type conductivity even in the absence of intentional doping. The reason is mostly attributed to nonstoichiometry. However, natural n type conductivity is not enough to make ZnO commercially usable. Lower resistivities can be achieved in two ways:

- Creation of intrinsic donors by lattice defects, like oxygen vacancies and/or Zn atoms on interstitial sites *(intrinsic doping).*
- Introduction of extrinsic dopant metals having three valance electrons on substitutional metal lattice sites or halogens with group seven on oxygen lattice sites in metal oxides *(extrinsic doping).*

Brief information about conduction mechanism of ZnO by means of intrinsic and extrinsic dopants are given below.

2.1.2.1. Intrinsic Dopants:

Mostly, ZnO was observed to show n type conductivity, even in the case of unintentionally doping. The origin of this was assumed to be *intrinsic dopants* in ZnO. *Intrinsic dopants* are natural defects that originate from deviations in the crystal lattice, away from stoichiometry.

The most commonly considered defect centers for ZnO are O vacancies (V_O), Zn occupying interstitial sites (Zn_i) and recently reported H occupying interstitial sites (H_i).

Which one of O vacancies (V_O) or Zn occupying interstitial sites (Zn_i) is the main souce of n type conductivity was researched (Suzuki, et al. 2001). Erthart, et al. assigned the zinc vacancy and the oxygen interstitials as acceptors (2006). According to them, Zn interstitials and oxygen vacancies acted as donors because they had shallow donor positions in the band gap. Depending on the growth atmosphere different defects are most likely: Under Zn rich conditions the oxygen vacancy dominates. In contrast, for an O rich atmosphere the Zn vacancy and the oxygen interstitials are the most likely defects. Taking the lower energy of formation of the Zn interstitial, was implicated that Zn_i it should be the dominant donor in zinc oxide. However, calculations indicate that its formation energy is too high to produce a concentration sufficient to account for the observed carrier concentrations. Modeling studies reveal that V_O is the most abundant defect, and its concentration was found to be quite similar to the carrier concentrations observed in single crystals (Lany and Zunger 2005). Like other wide-gap oxides, the neutral vacancy, V_O^0, however, is predicted to function as a deep level.

H_i has been found both experimentally and theoretically to be a shallow donor in ZnO, contributing to high carrier concentrations (Van de Walle 2000). In annealed materials, however, where H concentrations are reduced, elevated carrier concentrations can still be observed.

Under metal-rich, O-deficient growth conditions at high temperatures, free-carrier densities can be adjusted through the range of 10^{17} – 10^{20} cm^{-3} with O deficiencies commonly up to 1 at% (Wit 1975, Wit, et al. 1976, Halliburton, et al. 2005, Nakazawa, et al. 2006). Further extrinsic doping can produce densities in the range of 10^{21} cm^{-3} (Wager, et al. 2008).

The preparation of donor doped ZnO at high oxygen partial or annealing in oxygen atmosphere leads to highly resistive films. An explanation for this observation is

the formation of Zn vacancies owing to its low formation enthalpy under oxygen rich conditions. Since Zn vacancies are acceptors, they compensate the donors. Another explanation might be the oxidation of the corresponding metal (Ellmer, et al. 2008).

The lowest resistivity for (reactive) magnetron sputtered pure ZnO was observed to be $2x10^{-3}$ Ωcm with a carrier concentration of $1.2x10^{20}$ cm^{-3} and mobility of 16 $cm^{-2}/s/V$ (Webb, et al. 1981).

2.1.2.2. Extrinsic Dopants

Conductivity of ZnO can be increased by orders of magnitude via addition of small amounts of different valency metals. For example, adding group III atoms like Al, B, In or Ga results in n type doping. Especially Al is used for this type of doping. The lowest resistivity for Al doped ZnO obtained on the literature until today is $8.5x10^{-5}$ Ωcm (Agura, et al. 2003) and is grown by PLD (Pulsed Laser Deposition) technique. Lowest resistivities achieved with magnetron sputtering technique is $1.9x\ 10^{-4}$ and $2.7x\ 10^{-4}$ were reported by Minami et al (1984).

It is assumed that group III atoms are built in onto lattice sites. This means that metal atoms take the place of Zn in the lattice and uses 2 of its electrons for bonding the lattice. The third electron, not required for bonding joins the conduction band and contributes to conductivity (Ellmer, et al. 2008).

P type doping of ZnO is a hard goal to achieve. Known p-type dopants include group-I elements Li, Na, K; group-V elements N, P and As; as well as copper and silver. However, many of these form deep acceptors and do not produce significant p-type conduction at room temperature (Ozgur, et al. 2005). Current absence of p-type ZnO does limit its electronic and optoelectronic applications which usually require junctions of n-type and p-type material.

2.1.3. Optical Properties of ZnO

Similar with all semiconductors, optical and electrical properties of ZnO are determined by its band gap structure. The semiconductor is transparent to visible light due to its band gap energy. The process can be explained in terms of photon absorption by electrons. When light enters the semiconductor, the photons with energies higher

than band gap of the TCO are absorbed, which means that those photons can not pass through the semiconductor. However, the photons with lower energies than the band gap can not be absorbed, so they pass through the semiconductor, which makes it transparent for the wavelengths corresponding to those lower photon energies. Therefore, high optical transmission requires large band gaps (>3 eV).

In order to investigate the band structure, several methods are available. These methods basically measure the energy difference by inducing transitions between electronic levels such as transitions from the upper valence band states to the upper conduction band states and from the lower valence band states or by exciting collective modes (e.g., the upper core states to the lower edge of the conduction band and to excitations of plasmons). Another important method for the investigation of the energy region is based on the photoelectric effect extended to the X-ray region, namely, photoelectron spectroscopy (PES). The peaks in emission spectrum correspond to electron emission from a core level without inelastic scattering, which is usually accompanied by a far less intense tail region in the spectrum (Markoc, et al. 2009).

As mentioned before, ZnO is a wide band gap semiconductor with a band gap of 3.4 eV. It has direct band gap, which means that valance band maximum and conduction band minimum lies on the same wave vector k=0. Observations indicate that ZnO has O centered valance band and Zn centered character conduction band.

The optical and electrical properties of ZnO is controlled by 4s orbital of ZnO. It is a compound that contains metal ions with $4s^0$ and oxide anions with $2s^2 2p^6$ valance electron configurations.

When ZnO is ideally stoichiometric, the Fermi level is associated with filled O $2p^6$ valance bands and empty metal centered $4s^0$ conduction bands. However, real samples contain intrinsic or extrinsic defects that contribute to the production of charge carriers and placement of the Fermi level near or within the 4s conduction band, which results in n type transport.

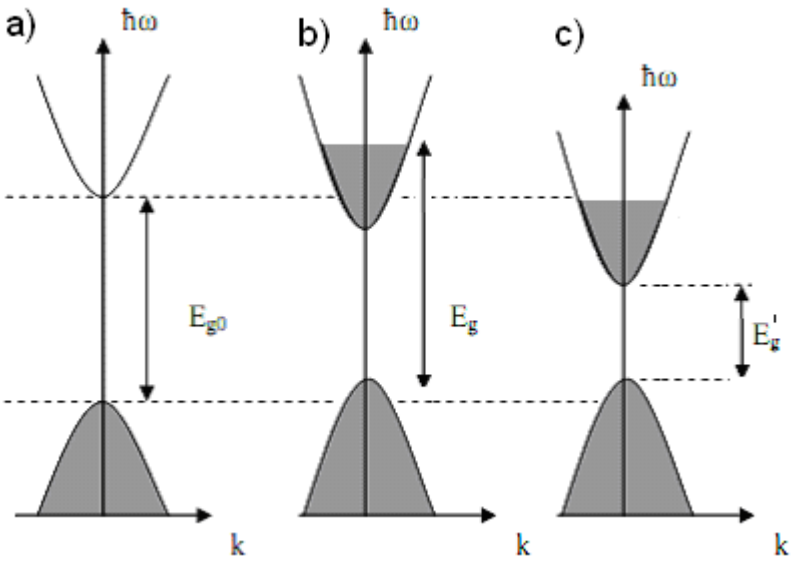

Figure 2.4. A simplified band gap description of TCOs: (a) without impurities, (b) band gap widening (c) band gap narrowing (Source: Bashar 1998).

The conduction band is curved upwards, the valence band is curved downwards and the Fermi level is located at mid bandgap for the undoped TCO (for our case ZnO) as shown in Figure 2.4.a. When doping concentration increases, bottom levels in conduction band are occupied. Because of Pauli's excursion principle, carriers on the upper levels of valance band can not be excited in the lower levels of conduction band. Therefore, carriers in deeper levels in the valance band have to be excited to upper levels in conduction band, resulting in increase of band gap from E_{go} to E_g (Figure 2.4.b). It is also observed that in degenerately doped semiconductors, coulombic interactions shift the conduction band downwards and the valence band upwards - effectively narrowing it from E_g to E_g' as shown in Figure 2.4.c. The bandgap increase by the Burstein-Moss shift is partially compensated by this effect (Franken 2006, Bashar 1998).

2.1.4. Scattering Processes

The mobility, therefore the conductivity of semiconductors is affected by several scattering processes. Here, the processes that occur in polycrystalline structures will be mentioned since this study includes this type of thin films.

The major scattering mechanisms that generally govern the electron transport in semiconductors are also valid for ZnO. They are briefly listed as follows:

(i) *Ionized impurity scattering* is due to deflection of free carriers by the long range Coulomb potentials of the charged centers caused by defects or intentionally doped impurities. This can be thought as a local perturbation of the band edge, which affects the electron motion.

(ii) *Grain Boundary Scattering (Dislocation scattering)* is mainly observed in polycrystalline films, since they include large amounts of crystallographic defects.

Polycrystalline material additionally allows oxygen to be physisorbed at the grain boundaries. Due to the higher electron affinity of oxygen, a grain boundary can be treated as a trap which acts like an acceptor and catches electrons. Captured electrons charge the grain boundary negatively and make it hard for electrons to pass through the grain. Therefore an energy barrier occurs which decreases the mobility of electrons. In order to lower the energy barrier, release of electrons from the barrier and neutralization of grain boundary is necessary. This can be accomplished by adding donor atoms in the structure. Taking into account these facts, it can be concluded that for lower doping levels, energy barrier is large, so that mobility is small because electros can not pass the energy barrier. As the doping density increases, the barrier decreases so that mobility, which is still dominated by grain boundary barrier-inhibited transport, will increase. However, once energy barrier becomes negligibly small, mobility will decrease with increasing doping density since ionized impurity scattering begins to dominate (Ellmer, et al. 2008).

The mobility therefore is dependent on the density of grain boundaries or the sizes of the crystals. The lowest resistivity will be obtained when all scattering mechanisms are eliminated. Therefore, the goal is to obtain a low resistivity with the lowest amount of charge carriers and the highest mobility (Franken 2006).

2.2. Advantages and Disadvantages of ZnO

Today, mostly used material for transparent conducting oxide applications is Indium doped Tin Oxide (ITO) owing to its low resistivity and high conductivity. However, the cost of ITO is increasing, because it is a rare material which is found in a restricted part of the earth e.g. China and likely to extinct in the near future. As FPD

(flat panel display) televisions, touch screen monitors and solar cells gets popular and popular, ITO seems to fail in covering the demand. Therefore new materials that would replace ITO are researched widely. Another item that pushes to look for new materials is the fact that ITO is toxic and is a threat for health (Gordon 2000). One powerful candidate is Al doped ZnO owing to its advantages that will be summarized in this section.

Firstly, low resistivities comparable to ITO are achieved with ZnO. The lowest resistivity on the literature until today obtained is 8.5×10^{-5} Ωcm (Agura, et al. 2003).

Secondly, as mentioned above, ZnO is an abundant material which is a fact that lowers the cost. To give an idea about the abundance of ZnO, following comparison would help: There is about 10.000 times more SnO and 100.000 times more ZnO than there is ITO. This means that if the entire indium supply would run out inside of a year, still there will be enough zinc oxide to last for 100.000 years (Suzuki 2009).

Impurity doped ZnO films are more easily etched by both acid and alkaline solutions than ITO films. This makes it harder to apply photolithography process with wet treatments. It is suggested that using low temperature enchants may decrease the etching rate (Wit 1975, Wit, et al. 1976, Halliburton, et al. 2005, Nakazawa, et al. 2006). High etching rate may become advantageous for other applications as well. One example is thin film solar cells, where milky ZnO films with a textured surface structure are needed. It is easier with ZnO films to produce such structures on relatively low temperature substrates than milky SnO_2 films (Nakata, et al. 1991, Mianami, et al. 1992). The use of milky AZO transparent electrodes for solar cells can produce an improvement in efficiency resulting from a light confinement effect (Minami 2005).

One disadvantage of ZnO is its susceptibility to humidity and temperature. This fact is not a problem for thicker films like 500nm which can be used for solar cell applications and they can show performance that is comparable to ITO. However, for films thinner than 100 nm which serves for FPD, susceptibility against temperature and humidity becomes an issue.

When used in solar cells installed in cold regions or hot deserts, zinc oxide transparent conductive films have not demonstrated any problems associated with resistivity to high or low temperatures. This showed that ZnO is capable of operating within varying temperature ranges. However, heat became a problem during deposition. The maximum temperature ZnO transparent conductive films can withstand during the deposition process is about 300˚C, which is quite low when compared with 400˚C for

ITO films and 500˚C for tin oxide films. Anyhow, this problem is overcome with improvements in sputtering conditions, furthermore became an advantage of ZnO. Owing to its availability to be grown at low temperatures, ZnO can be deposited on flexible substrates like plastics.

The most significant advantage of ZnO transparent conductive films is that they have better optical properties than other materials (Suzuki 2009). They have a better white balance when used in FPDs and other display devices. ITO has a slightly yellowish color, which can make colors appear less vivid. ZnO transparent conductive films, on the other hand, look bluish. This is a major plus since to the human eye blue makes white appear even more clearly.

One other advantage of ZnO is its radiation hardness to MeV proton irradiation which makes it an ideal candidate for solar cell applications (Look, et al. 1999).

2.3. Applications of ZnO

Although electrical and optical properties of ZnO are widely researched today, ZnO is very widely used in our society and is a key element in many industrial manufacturing processes. Some examples are paints, cosmetics, pharmaceuticals, plastics, batteries, electrical equipment, rubber, soap, textiles, and floor coverings (Coleman and Jagadish 2006).

Zinc Oxide (ZnO) is emerging as a material of interest for a variety of electronic applications. At present, the most widely publicized application for ZnO is as an ITO replacement for displays and photovoltaic panels, where ZnO could lower costs of transparent conductors, as mentioned above. However, new applications for ZnO cover a much broader area than that.

One of the most popular areas ZnO is utilized today is as transparent conducting oxides, which are used as transparent electrodes. ZnO is used as the front contact of solar cells, where the light enters the device which is also the application this study serves for. It both allows the light pass to the absorption layer without much loss and extracts the photocurrent.

ZnO is employed for many applications in electronics like flat screen displays, field emission sources, gas, chemical (Nakata, et al. 1991) and biological sensors, and as UV light emitters and switches (Nakata, et al. 1991, Minami, et al 1992, Moon, et al.

2007, Dingle, et al. 1978), coating UV and contacting LEDs and OLEDs (Coleman and Jagadish 2006). ZnO may also find applications in thin-film batteries.

Thin films of zinc oxide (ZnO) received much attention due to their unique piezoelectric and piezooptic properties, rendering them suitable for surface acoustic wave devices (Brooks 1955), low loss optical waveguides and modulators (Brooks 1951), optoelectronic devices (Jenkins, et al. 1997, Juares, et al 1998) and piezoelectric sensors (Weiher and Ley 1966). Emerging field for SAW devices are sensors in automotive applications (torque and pressure sensors), medical applications (chemical sensors), and other industrial applications (vapor, humidity, temperature, and mass sensors). Advantages of acoustic wave sensors are low costs, ruggedness, and a high sensitivity (Ellmer, et al. 2008)

Another prospective application of zinc oxide is the alloying with magnetic atoms like manganese, cobalt, or nickel to prepare diluted magnetic semiconducting alloys that are interesting as materials for spintronics, promising the possibility to use the spin of the electrons for electronic devices (Satoh, et al. 2004).

As for bulkier application areas, a large fraction of the ZnO is used in the rubber and concrete industries (Conwell and Weisskopf 1950). ZnO is an important additive to the rubber of tires of cars. It has a positive influence on the vulcanization process and it improves considerably the heat conductivity that is crucial to dissipate the heat produced in the rubber of the tire by the deformation when it rolls along the street. In concrete production, an admixture of ZnO allows increased processing time and improves the resistance of the concrete against water. Other applications concern medicine or cosmetics. ZnO is used as a UV-blocker in sun lotions or as an additive to human and animal food.

2.4. Deposition Methods of ZnO

Deposition method and conditions are one of the main items that plays role on the properties of the films. Some methods that gives resistivity results on the order of 10^{-4} Ωcm are vacuum arc plasma evaporation (VAPE), metal organic molecular beam deposition (MOMBD) (Sato, et al. 1993) and metal organic chemical vapor deposition (MOCVD) (Gordon 2000) as well as by magnetron sputtering (MSP) (Minami 1984, Minami 1999) and pulsed laser deposition (PLD) (Suzuki 1996).

Among the techniques above, plasma assisted processes which are PLD and magnetron sputtering lead to the lowest resistivity films because these methods do not only rely on thermal activation of the growth process, they also host the additional energy input from energetic particles like ions, sputtered particles, energetic neutrals. These methods result in films with better crystalline and electronic quality and they allow low temperature production (Ellmer, et al. 2008).

It has been reported on the literature that resistivities of films deposited by PLD are smaller than the ones deposited by magnetron sputtering. This is related to growth with better crystalline qualities. Higher Hall mobilities for approximately same carrier densities are possible in better crystallized films. This results in less grain boundary scattering, leading to higher mobility and lower resistivity. Another reason is it is easier to prevent oxygen from the environment in PLD. Also Zn is more chemically active with oxygen due to the low binding energy between Zn and O. Therefore in other techniques than PLD, the oxygen amount in the environment must be controlled precisely.

Despite availability of good quality film preparation, fabrication films on large substrates with high deposition rates are an issue with PLD which limits its industrial application. MOCVD is used for industrial applications; however, this process requires high substrate temperatures above 150 C^0 which is not suitable for all cases for thin film solar cells and for plastics substrates (Ellmer, et al. 2008).

When compared to other deposition techniques such as evaporation, chemical vapor deposition, spray pyrolysis or PLD, magnetron sputtering has several advantages such as availability to low substrate temperatures down to room temperature, good adhesion of films on substrates, high deposition rates (up to 12 μm min^{-1}) (Coleman 2006), very good thickness uniformity and high density of films, good controllability and long-term stability of process, availability for deposition of alloys and compounds of materials with very different vapor pressures. Also by reactive sputtering in rare/reactive gas mixtures compounds can be deposited from elemental metal targets which is relatively cheap. Scalability to large areas is an other advantage (Ellmer, et al. 2008) These advantages make ZnO to be referred as the conventional fabrication technique used today. Further information about the technique will be introduced in Chapter 3.

CHAPTER 3

EXPERIMENTAL DETAILS

In this study, experiments aiming to investigate the structural, electrical and optical properties of transparent and conducting Al doped ZnO thin films were performed. Radio Frequency Magnetron Sputtering (RFMS) and Direct Current Magnetron Sputtering (DCMS) is employed for the deposition of the films. Each film is deposited on both SiO_2 and 1x1 cm microscope slides.

Properties of the films were investigated by four point electrical measurements, X-Ray Diffractometer (XRD), UV Spectrometer, Atomic Force Microscope (AFM), Surface Profiler and Scanning Electron Microscope (SEM).

This chapter involves experimental details about the study and consists of two main parts. In the first part, preparation of samples including sample cleaning and thin film deposition is explained. In the second part, characterization techniques that are employed for structural, electrical and optical characterization are introduced.

3.1. Sample Preparation

Samples preparation process consists of sample cleaning process and thin film deposition. Films are deposited on 1x1 cm SiO_2 wafers and 1x1 cm glass samples. Samples are subjected to a cleaning process prior to films growth.

3.1.1. Sample Cleaning Process

In order to achieve better results, it is crucial to prevent samples from contaminations. In the process, firstly glass substrates were rinsed in acetone, dried by rubbing with a piece of tissue and then nitrogen was blown on them in order to get rid of the dust remained from the tissue. Following that, both glass and SiO_2 substrates were rinsed in acetone for 10 minutes in ultrasonic bath. Than they were rinsed in propanol

(isopropyl alcohol) and dried with nitrogen. Before inserting the samples into the loading chamber, they were blown nitrogen again.

After the cleaning process, a line of photoresist was put onto the samples. After deposition, this photoresist is removed and thicknesses of the films were measured by measuring the step height between the substrate and the film surface via AFM or surface profiler.

3.1.2. Thin Film Deposition

Films for this study were deposited by using "Magnetron Sputtering Technique (MS)". Sintered ZnO and metallic Al targets were used. ZnO is deposited by RF magnetron sputtering, whereas Al was deposited by DCMS technique. Details about the techniques are presented below.

3.1.3. Magnetron Sputtering Technique

Magnetron sputtering (MS) is a widely used film deposition technique with a large number of advantages. It belongs to the family of physical vapor deposition techniques. Its principle relies on sticking of removed target atoms onto a substrate.
Figure 3.1 illustrates the sputtering process, which can be summarized as follows:
Low pressures of Argon atoms on the order of 10^{-3} Torr are fed into the chamber. Ar atoms are ionized as a result of collisions with electrons. Then these ions are accelerated towards negatively charged target material (cathode) by means of electric and magnetic field. The magnetic field strength is adjusted in such a way (about 50 to 200 mT) that the electrons are significantly influenced by the magnetic field while the ions are not (Ellmer 2000). When they hit the target material, they remove atoms from target as a result of momentum transfer from large Ar^+ ions to target material. Positive ions recombine with removed electrons and return to their ground states. During this, they release energy in form of photons which is the result of the glowing appearance of the plasma. Removed target atoms are free of charge, so they are not affected by magnetic or electric field and can move towards the substrate and begin to form desired films. Electrons follow a cycloidal orbit in the crossed electric and magnetic fields around the

target, therefore their chance of ionizing Ar atoms, therefore duration of the plasma increases.

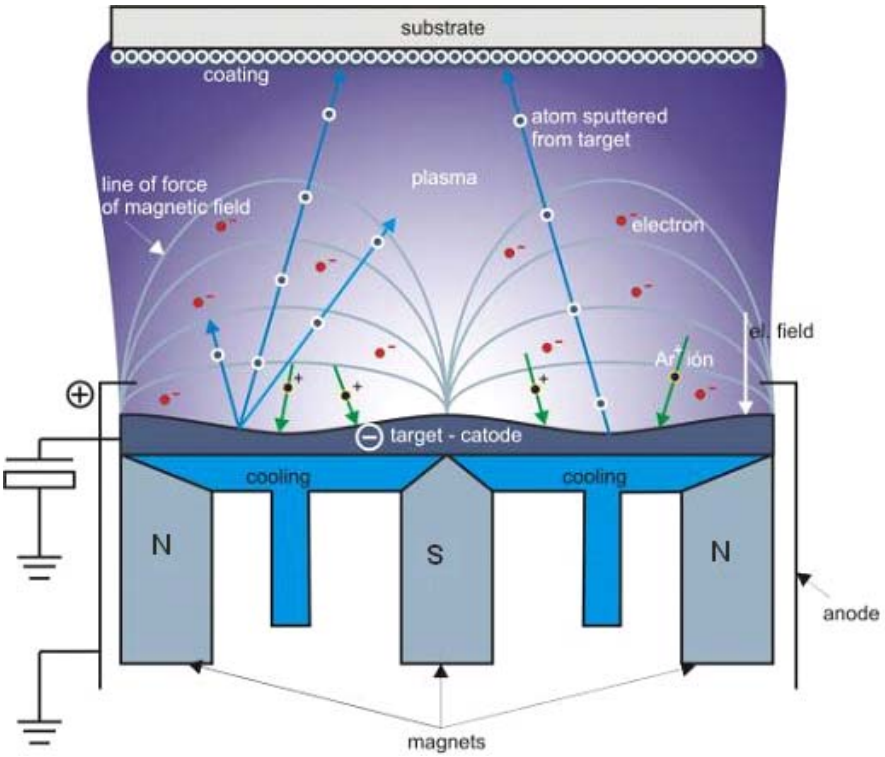

Figure 3.1. Illustration of magnetron sputtering process.
(Source: Slovak Academy of Sciences 2006)

Most common magnetron sputtering techniques are DC, RF and Reactive Magnetron sputtering. These techniques owe their names to the power supply that is used for discharge.

3.1.3.1. DC Magnetron Sputtering

In DC MS, the discharge, namely plasma is formed with a DC power supply. The dc discharge is based on the generation of ion-induced secondary electrons at the target. Therefore, large target voltages are necessary to sustain the plasma because the electron emission increases almost linearly with the ion velocity. As a consequence of this, discharge voltage (the negative dc voltage that is measured at the target) is much lower for rf compared to dc excitation. Metallic targets are mostly sputtered by DC

power supplies whereas charge build up problem is observed in insulator targets. Collisions of ions with the target material remove electrons from the target as well; therefore some positive charge may build up on the target. This effects sputtering process negatively because positive charge built prevents Ar^+ ions hit the target. This effect which is observed in insulator targets can be overcome by RF magnetron sputtering.

3.1.3.2. RF Magnetron Sputtering

In insulating targets, positive charge builds up on the target and prevent Ar^+ ions hit the target. Therefore large DC voltages around 10^{12} Volts are required to sputter insulators. The rf plasma is mainly driven by ionization due to electrons which perform an oscillating motion in the plasma. At frequencies less than about 50 kHz, both electrons and ions in plasma are mobile and both can follow the switching of the anode and cathode which results in basically DC sputtering of both surfaces. On the other hand, at frequencies above about 50 kHz, ions (heavy) can no longer follow the switching and electrons can neutralize positive charge build up. Furthermore, when electrons move back and forth in the plasma, their chance of hitting Ar atoms and ionizing them increases. This kind of excitation is much more effective compared to the ionization by non-oscillating secondary electrons and leads to lower target voltages in an rf discharge. The low discharge voltages lead to significantly lower deposition rates for an rf magnetron discharge compared to a dc sputtering process under the condition of constant discharge power (Ellmer 2000).

3.1.3.3. Reactive Magnetron Sputtering

For many thin film applications, compound films like oxides such as ZnO are necessary as in the case of this study. If it is desired to grow compound films like oxides, RF MS from ceramic targets is one way to produce them. However ceramic targets are fragile and more expensive compared to elemental targets. One way to decrease cost is to use cheaper elemental targets e.g. metallic targets and do sputtering in an atmosphere of argon and a reactive gas, like oxygen. The reactive sputtering

process is a very attractive method since it is possible to produce layers with different chemical composition and hence properties by varying the reactive gas partial pressure. Furthermore, the deposition rates are generally higher compared to deposition from a compound target. Another advantage is the possibility of using dc power supplies. Ceramic compound targets are often too insulating to be sputtered by dc excitation. In this case rf power supplies have to be used, which are much more expensive than dc supplies. However, reactive sputtering often requires careful process control since the desired layer properties can only be obtained within a narrow parameter window. It should be noted that reactive sputtering can poison target if chemical reactions are faster than sputter rate.

In our study, we deposited the films by Radio Frequency (RF) Magnetron Sputtering and Direct Current (DC) Magnetron Sputtering. Sputtering was performed with ATC Orion 5 UHV Magnetron Sputtering System with a sputter-up orientation (Figure 3.2). System was controlled with computer which helps obtaining identical parameters during repeating experiments. The system had 5 AJA-International sputtering guns, 2 RF (13.56 MHz, max power 500W), 3 DC (max power 300W) power supplies. Shutters over the targets made it possible to deposit one or more materials at the same time. On the substrate holder, a halogen lamp which can heat up the sample holder to 850^0C for substrate heating was attached. In addition, substrate holder could be rotated up to a speed of 100 rpm enhancing uniform deposition. The system had a load chamber with a magnetic transfer arm which gave the advantage to insert substrates to the main chamber without breaking UHV. Each chamber was pumped with a turbo pump assisted by a rough pump. The base pressure and working pressure were 4.2×10^{-7} Torr and 3 mTorr respectively.

Figure 3.2. ATC Orion 5 UHV Magnetron Sputtering System

3.1.4. Growth Procedure

Films were deposited by magnetron sputtering by codeposition from ZnO and Al targets as shown in Figure 3.3. Sputtering gas was Ar. Substrates were cleaned before deposition as told before. ZnO was sputtered with a RF power source, whereas Al was sputtered from a DC power source. The base pressure was 4.2×10^{-7} mbar and working pressure was 3 mTorr. Substrate- target distance was kept constant approximately 10 cm. The samples were rotated with a speed of 70 rpm in order to obtain uniform film thickness.

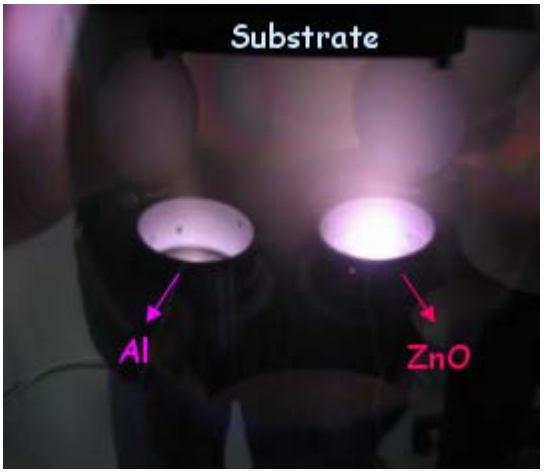

Figure 3.3. Codeposition of ZnO and Al.

Firstly, experiments aiming to optimize sputtering parameters of pure ZnO were performed. 60, 120 and 180 W were used as deposition power. During deposition with 120 W and 180 W, it was observed that plasma was flashing; indicating that shorts were occurring at ZnO target and plasma was unstable. Therefore 60 Watts was chosen as deposition power. Deposition time was 30 minutes for all samples. Once sputtering power, sputtering time for pure ZnO films were selected; those films were doped with Al. Effect of decreasing Al content was investigated. Al concentration of the films was decreased in three steps:

1. Al power was decreased from 20 to 2.5 W.
2. A method named "*modulation doping*" was employed. (Ellmer and Vollweiler 2006, Digle, et al. 1978, Joshua and Wolden 2003, Rauf 1993)
3. Modulation doped film with the lowest resistivity was deposited again by applying substrate bias with powers of 20, 10 and 5.

Modulation doping was introduced by Dingle, et al. (1978) for GaAs/GaAlAr multilayers. It is also used for heavily doped TCO films (Ellmer and Vollweiler 2006, Joshua and Wolden 2003, Chopra, et al. 1983).

In modulation doping, dopants are implemented in such a way that the resulting free electrons are spatially separated from the positive donor ions. By this way, ionized impurities remain in heavily doped region, while electrons transport in undoped region.

This leads to higher mobility with the same amount of carrier concentration. Robins, et al. (2003), Dingle, et al. (1978), Ellmer and Vollweiler (2006) deposited periodic stacks of highly doped and undoped layers. In these structures, layer of high doping concentration acted as supply of carriers, whereas low doping concentration layer acted as transport layer. Carriers from high concentration region segregated into transport layer as a result of a potential originated from band gap difference of layers. As illustrated in Figure 3.4. Mobility of modulated doped structures was higher because carriers could move more effectively in low doping concentration layer due to significantly less ionized impurity scattering. By the help of the method, high mobility and conductivity can be achieved with thinner films leading to higher optical transmission values still maintaining low sheet resistance. However, Ellmer (2001) predicted the resistivity of modulation-doped layers would be limited to 1.5×10^{-3} Ωcm since the transferred maximum electron sheet density is only about 10^{13} cm^{-2}.

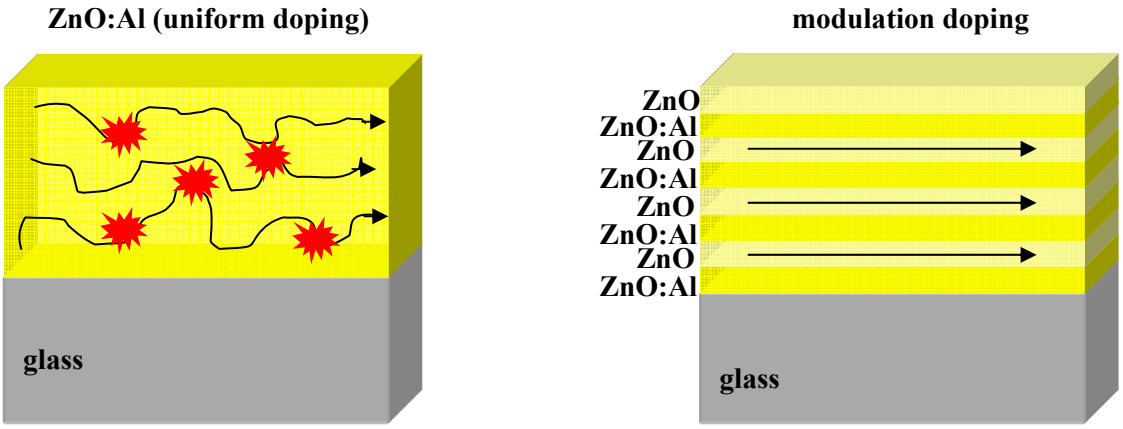

Figure 3.4. Illustration of carrier transport in uniformly and modulation doped structures.

In his study, Ellmer and Vollweiler changed the thickness of both transport and doping layers (2006). Different from him, in our study, we changed the thickness of only transport layer (pure ZnO) while keeping total deposition time constant. This resulted in films of nearly the same thickness but with thicker transport layers, therefore less Al content.

It is known that in order that the modulation doping principle works, the thickness of the multilayers has to be in the range of the penetration depth of electrons to achieve a sufficient carrier transfer from the doping to the transport layer (Wager, et al 2008). This means that the thickness of pure ZnO layer should be less than 5 nm in order to avoid intersubband scattering (Cohen and Barnett 2005). Therefore, in this study, we used ZnO stacks of grown for 0.5, 1, 1.5, 2 and 3 min (estimated thicknesses are ~0.5, 1, 1.5, 2, 3 nm).

We performed modulation doping by means of depositing periodic stacks of pure ZnO and Al doped ZnO. Pure ZnO layer corresponded to transfer layer whereas Al doped ZnO layer corresponded to doping layer. ZnO shutter was open during whole growth of the samples whereas Al shutter was opened and closed periodically in order to form doped layers. Deposition parameters of pure ZnO layers and Al content of doped layers were kept constant for all samples. In individual samples, all doping layers and the transport layers were the same thick. The thicknesses of the undoped layers

were varied from sample to sample by changing the duration time that Al shutter was closed.

Once we received the lowest resistivity results with modulation doping method, in order to decrease the resistivity further, we applied bias to substrate. We thought that this might decrease the growth rate and decrease Al content. Addition to this, we thought that this method would lead to smoother interfaces. We applied RF bias powers of 5, 10 and 20 W to substrates.

All the films are subjected to post annealing treatment at 300^{o}C in vacuum. We thought that this might improve crystal structure of films and decrease resistivity.

CHAPTER 4

RESULTS AND DISCUSSION

This chapter consists of 5 main parts. In the first part, results about the properties of pure ZnO are given. In the second and third part, results about effect of Al content on the properties of the films are reported. The second part involves decreasing of Al content by decreasing power of Al, while third part investigates further decreasing of Al content by layered growth (modulation doping). Effect of applying bias to substrates is given in the fourth part and in the final part; effect of post deposition annealing is discussed. In each part, results on structural, electrical and optical characterization are presented. Employed structural characterization techniques were XRD, AFM, SEM and surface profiler. Optical characterization was performed by UV spectrometer between wavelengths 200-900 nm.

Information on surface structure and thicknesses of some samples are obtained by AFM, surface profiler and SEM. Thicknesses of some samples were estimated from growth rate (measured by calibrated thickness monitor) and deposition time. Resistivities of the samples were obtained by four point measurements.

4.1. Properties of Pure ZnO

Prior to investigating properties of Al doped films, properties of pure ZnO films were studied in order to define parameters of ZnO to be used for the rest of the study. Deposition power, deposition time, therefore thickness of ZnO was adjusted in the first place. 60 W, 120 W and 180 W were tried as deposition power. In depositions with 120 W and 180 W, it was observed that plasma was flashing; indicating that shorts were occurring at ZnO target and the plasma was unstable. When chamber was opened, it was seen that flakes had occurred on the surface of ZnO. It was understood that these flakes were the cause of the shorts. Therefore 60 W was chosen as deposition power of ZnO at the rest of the study to prevent damaging the target and to obtain stable plasma. Each film was deposited both on 1.25 mm thick glass and 400 μm thick SiO_2/Si substrates.

Samples were rotated with a speed of 70 rpm during deposition. Deposition parameters of films are listed in Table 4.1.

Table 4.1. Deposition parameters of pure ZnO samples.

RF Power (W)	Pressure (mTorr)	Sputtering Time (min)	Thickness (nm)
60 W	3 mTorr	15 min	20 nm
60 W	3 mTorr	30 min	30 nm
60 W	3 mTorr	60 min	75 nm
60 W	3 mTorr	90 min	110 nm

4.1.1. Characterization of Pure ZnO

Surface roughness, thickness, crystal orientation, grain size, resistivity, optical transmission and the band gap of pure ZnO samples were investigated.

4.1.1.1. Resistivity of Pure ZnO

Sheet resistance of pure ZnO films was measured by 4 point probe technique with Keithley Model 2420 sourcemeter instrument. However their sheet resistance was out of the measurement range of the instrument (R>21.1 MΩsq).

4.1.1.2. Thickness and Roughness of Pure ZnO

In order to have low resistivity films, surface roughness should be low because it leads to increment of resistivity due to scattering from rough surfaces. Also fabricating smooth surfaces would lead to smoother interfaces. Since, smooth surfaces require optimum deposition power. Because very high deposition power would lead to higher deposition rates and when rate is high, atoms do no have sufficient time to migrate on the surface to form smooth and good textured films. On the other hand, if deposition

power is too low, target atoms would not have enough energy to adhere on the surface. Even if they adhere, they would not have sufficient energy to migrate and this, again, would result in rough films. Therefore, firstly a deposition power was chosen and corresponding deposition rate was identified. ZnO deposition parameters are given on Table 4.1.

Thicknesses of the films are measured by AFM and profilometer. Result is presented in Figure 4.1. Deposition rate was accepted to be 1 nm/min for pure ZnO.

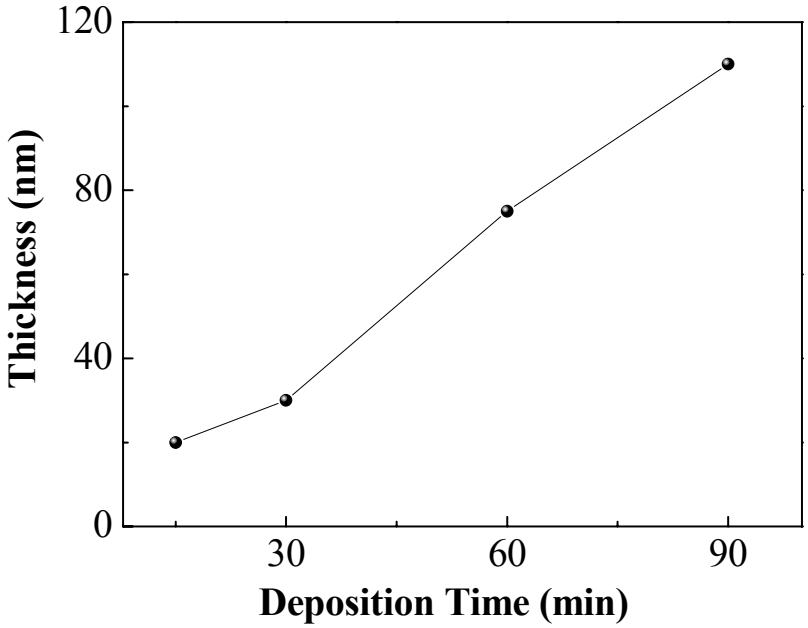

Figure 4.1. Thickness vs deposition time plot for pure ZnO on glass substrates.

Thickness and root mean square roughness (RMS Roughness) of the films were measured by AFM. Results showed that roughness of films deposited both onto SiO_2/Si and glass substrates were about 2.5 nm (Figure 4.2). It was seen that roughness of films deposited on glass substrates was higher than the films on SiO_2/Si substrates. This can be attributed to smoother surface of SiO_2/Si substrates compared to glass substrates. For glass substrates, roughness was increasing with thickness, whereas for SiO_2/Si substrates it was fluctuating in a narrow RMS range. It was seen that thickness for 30 min film was ~30 nm. 30 min was chosen as thickness parameter of ZnO for the rest of the study.

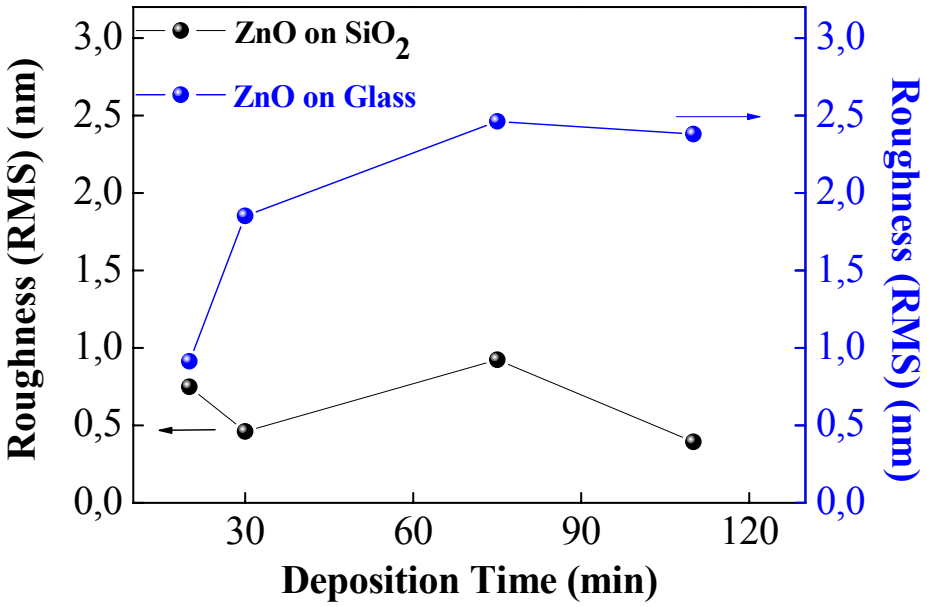

Figure 4.2.Roughness values for ZnO films on glass and SiO_2/Si substrates.

4.1.1.3. XRD Results of Pure ZnO

When there are very intense peaks (e.g. from substrate) in any spectral measurement, less intense peaks may be washed out and could not be determined. In order to fix this problem, Grazing Incidence XRD (GIXRD) is used. Crystal structure of the films was investigated by GIXRD technique by using Philips X'Pert PRO MRD (multi-purpose X-ray diffraction) system assisted with X'Pert High Score Software.

GIXRD uses small incident angles for the incoming X-ray so that diffraction occurs mostly on the surface. It is used to study surfaces and thin layers in the order of nanometers. When material studied is exposed to X-rays, an evanescent wave is established for a short distance and is exponentially damped. Therefore Bragg reflections are only coming from near surface structure. This technique gives the chance to eliminate strong peaks from substrate. The small angle that achieves elimination of intense peaks is called "critical angle". Critical angle for glass and SiO_2/Si substrates are defined to be 0.35^0 and 0.30^0 respectively. The obtained data from GIXRD measurements are given in Figure 4.3.

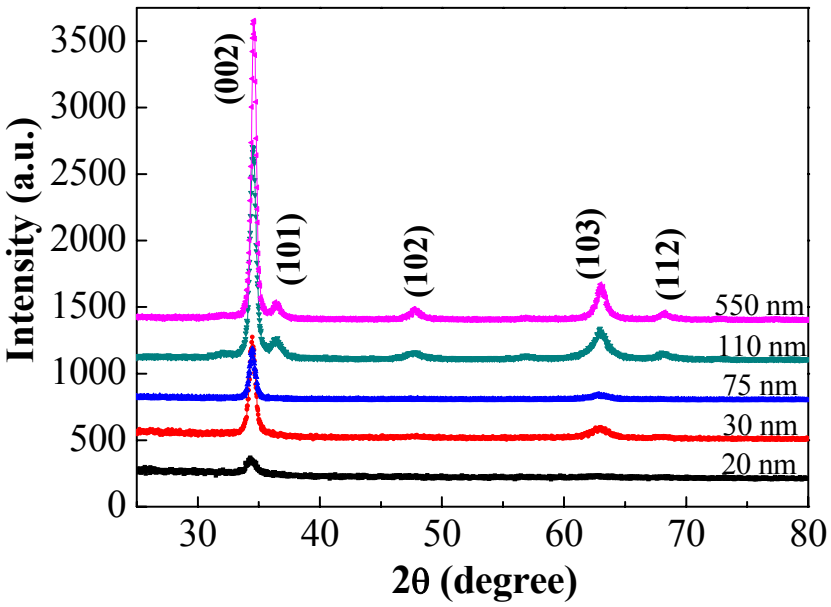

Figure 4.3. XRD results for pure ZnO films of various thicknesses grown on glass substrates.

It was observed that ZnO films were polycrystalline and mostly textured in (002) direction. Crystallization towards (002) indicated that our films were c-type ZnO grown in polar direction (Caihong, et al. 2008).

The ZnO (002) peak was observed even in the thinnest film. As the thickness of the films increased, crystal peaks in other directions such as (101), (102), (103) and (112) were also observed, indicating that for higher thicknesses growth in other directions reached to observable amounts.

Grain size of the crystallites in (002) direction was calculated via X'Pert High Score software by Scherer's formula:

$$D = \frac{0{,}9\lambda}{\beta \cos\theta} \tag{4.1}$$

where λ is x-ray wavelength (1.54 $\mathring{A}$), θ is Bragg's angle, and β is the full width of diffraction peak at half of the maximum intensity. When measuring FWHM, firstly background was subtracted, than each peak was zoomed in and profile fitting was

performed. Relationship between grain size of ZnO (002) peak and film thickness is given in Figure 4.4. The inset shows FWHM values corresponding to (002) peak.

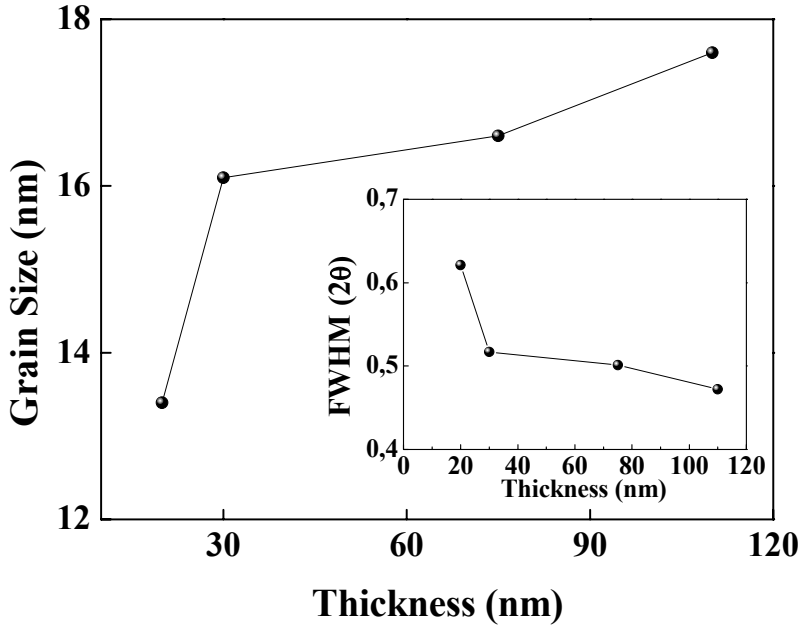

Figure 4.4. Grain size of ZnO (002) peaks of films with various thicknesses. Inset shows FWHM vs films thickness.

It can be seen on Figure 4.4 that beginning from 30 nm thickness, grain size of (002) peak increased almost linearly while FHWM value decreased. Smallest grain size of about 13 nm was observed in the thinnest film. This result might be expected because grain formation may not be completed at such small thickness. Maximum grain size of 17.6 nm was observed in 110 nm films. Grain size of films with the thickness of 30 nm, was about 16 nm.

Figure 4.5 shows variation of lattice strain due to increasing thickness. The strain was calculated by Scherrer calculator in X'pert software with the formula

$$\varepsilon = \frac{\beta}{4\tan\theta} \tag{4.2}$$

where β is the full width of diffraction peak at half of the maximum intensity and θ is Bragg's angle.

It was seen that strain was released with increasing thickness. When there is mismatch between the substrate and the film, some energy accumulates, causing strain

in the film. As the thickness increased, extra energy was released by formation of lattice defects. Release of energy causes decrease in lattice strain. Same effect was also assumed to be the increase in grain size.

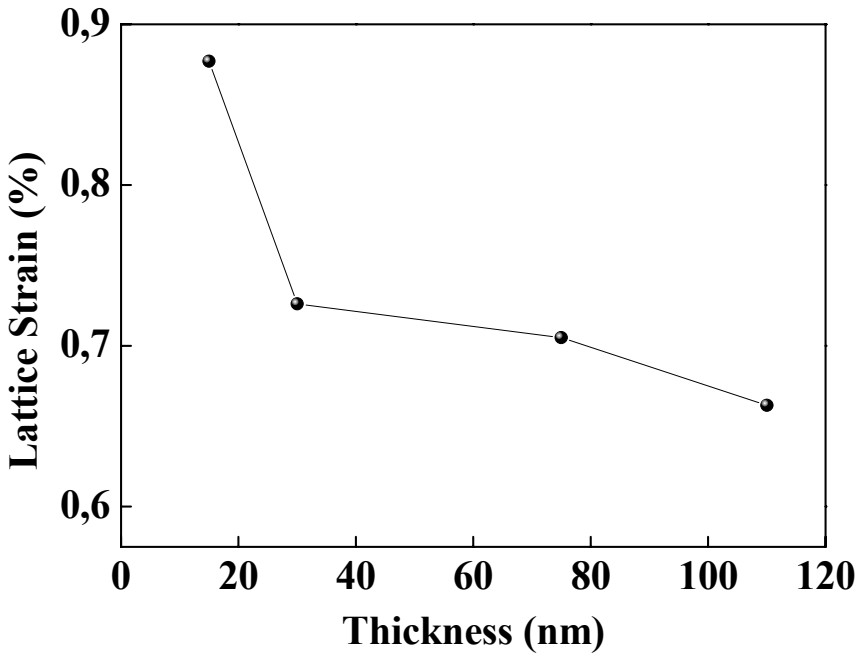

Figure 4.5. Lattice strain of ZnO (002) peaks of films with various thicknesses.

4.1.1.4. SEM Results of Pure ZnO

Surface of pure ZnO films was smooth and did not show grainy structure Surface of 20 nm (15 min) film is shown in Figure 4.6.

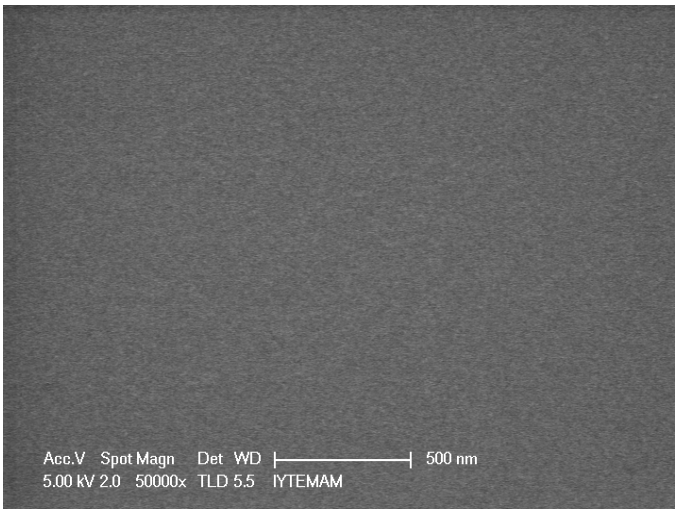

Figure 4.6. SEM image of 20 nm ZnO.

Figure 4.7 shows cross sectional SEM image of pure ZnO. To emphasize the growth structure, picture of about 650 nm thick pure ZnO film is given. Columnar structure of the film can be seen clearly.

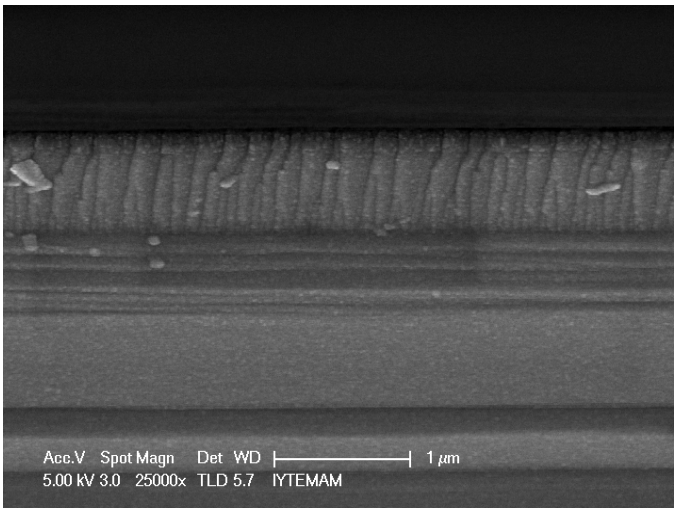

Figure 4.7. Cross sectional SEM image of ZnO.

4.1.1.5. Transmission Results of Pure ZnO

Transmission spectrum of the samples was measured by Varian Cary 50 Scan Visible Spectrometer between wavelengths of 200-900 nm. Before taking the measurements, background correction was performed by measuring the transmission

spectrum of air. After air was assigned as baseline, transmission spectrums of the samples were taken. This means that obtained data was transmission spectrum of glass-film structure. Transmission of glass substrates was measured as reference as well. Obtained data of ZnO films grown on glass substrate with various thicknesses is given in Figure 4.8.

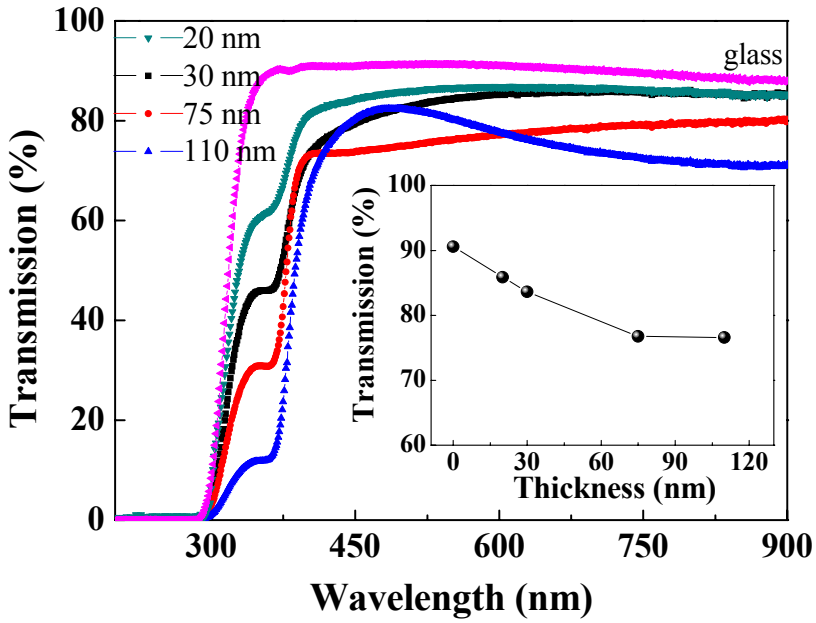

Figure 4.8. Transmission data of pure ZnO films of various thicknesses on glass substrates. Inset shows average transmission of the films between wavelengths of 400-800nm.

It was seen that transmissions of the samples were decreasing as the thicknesses of the films were increasing. It was assumed that increase of film thickness increased scattering, refection and optical absorption on the film surface (Jeong and Park 2002).

Before absorption edge, a dip was observed in the transmission spectrum of pure ZnO films. As the thickness was increasing, height of the dips were decreasing. The reason of these dips was attributed to two possibilities. First possibility was interference between air/ZnO/glass dielectric interfaces (Muth, et al. 1999). Decrease of height of the dips was attributed to reflections between the interfaces. Second possibility was thougt to be due excitations of electrons from lower levels of valance band to condction band (Dekkers 2007).

Fluctuations in transmission spectrum began to occur with increasing thicknesses owing to interference effects. Such fluctuations were observed in the

literature with films thicker than 200 nm as well (Lee and Song 2008, Schropp, et al. 1988).

Average transmission of the films were calculated by taking average of the transmission values between wavelengths 400-800 nm and the result is shown in the inset of Figure 4.8. Transmission for all thickness values is higher than 70%. Transmission of 30 nm thick film is 84% and is close to transmission of substrate (glass) which is 91%. It is known that decrease in grain size results in the light scattering losses and the destruction of coherence between incident light and reflected light, leading to the disappearance of interference fringes as well as the decrease in transmittance (Bai and Tseng 2009).

4.1.1.6. Band Gap of ZnO Films of Pure ZnO

Band gap of the films are defined by using their transmission data. Relationship between T, R and α is as follows (Kerkache, et al. 2006):

$$T - R = e^{-\alpha t} \tag{4.3}$$

where T and R are transmission and reflection values, α is absorption coefficient and t is the thickness of the film. Since R is very small for films with transmission over 80%, it can be neglected (Kerkache, et al. 2006). Thus, the equation becomes

$$T = e^{-\alpha t} \tag{4.4}$$

$$\alpha^2 = \frac{[\ln T]^2}{t^2} \tag{4.5}$$

It is known that for semiconductors with a direct band (Pankove 1975),

$$\alpha h\nu = (T - R)(h\nu - E_g)^{1/2} \tag{4.6}$$

$$(\alpha h\nu)^2 = (T - R)^2 (h\nu - E_g) \tag{4.7}$$

where α is absorption coefficient, T and R are transmission and reflection values for photons with energy (hν), h is Planck constant, ν is the frequency of the photon and E_g is the band gap energy. If R is neglected as discussed before, the equation above becomes

$$(\alpha h\nu)^2 = T^2(h\nu - E_g) \tag{4.8}$$

It can be seen from this equation that when α^2 is zero, the energy of the photon corresponds to band gap energy. In other words, the energy of photons that can excite from valance band to conduction band without being absorbed has the energy equal to band gap energy. Therefore, when α^2 vs hν graph is extrapolated, the x intercept refers to the band gap energy.

Extrapolation of α^2 vs hν graph for pure ZnO films are given in Figure 4.9. It was observed that there were two absorption regions: one at around 4 eV, other at about 3 eV. Figure 4.10 is given to show the absorption about 3.2 eV more clearly. The small absorption energy was due to dips in the transmission spectrum (Figure 4.8). (In the spectrum, there were dips at about 400 nm implying referring to absorption of energies about 3 eV). Corresponding band gap values obtained from Figure 4.9 and Figure 4.10 are given in Figure 4.11.

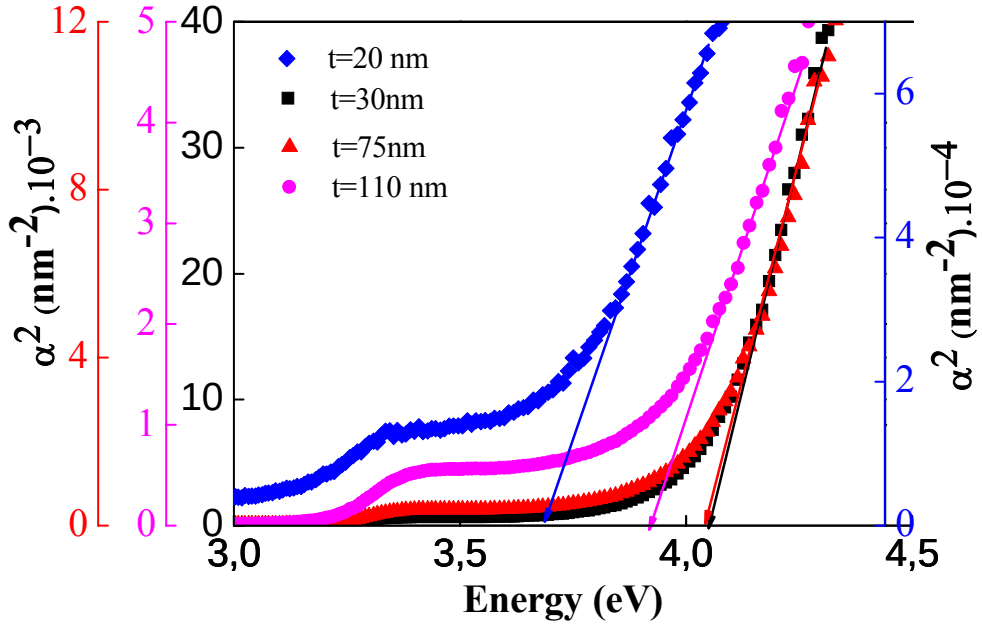

Figure 4.9. Extrapolation for defining band gap of pure ZnO films.

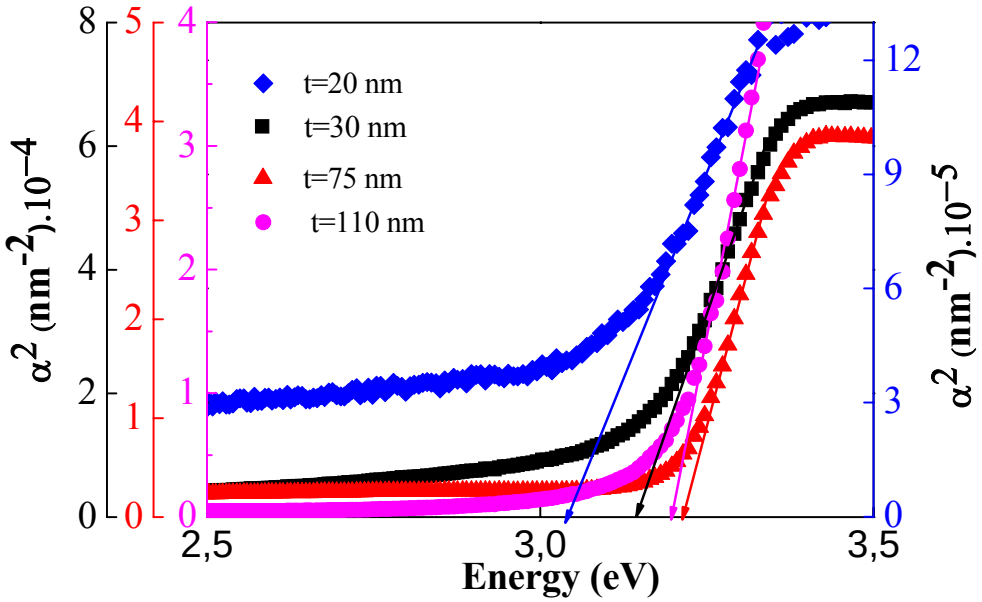

Figure 4.10. A Closer look into Figure 4.9 between energies 2.5 and 3.5 eV.

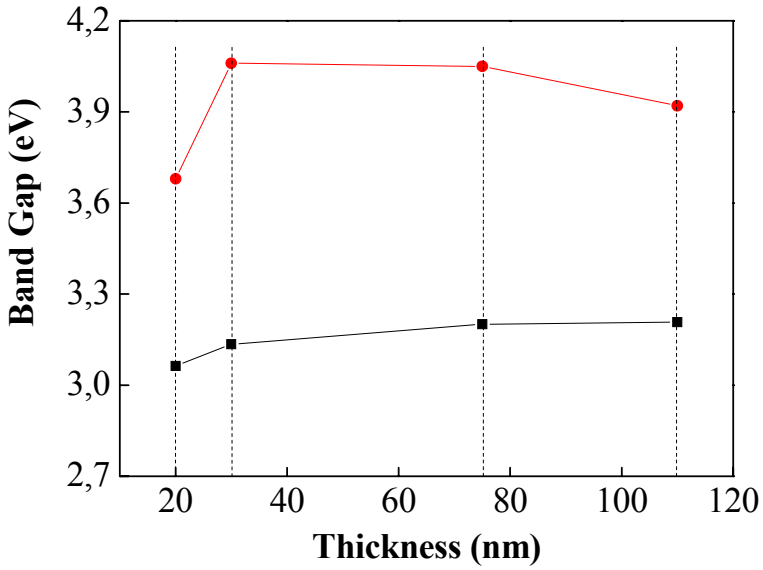

Figure 4.11. Absorption energies of pure ZnO with various thicknesses.

Figure 4.11 shows both absorption energies obtained from Figure 4.10 (red points) and 4.9.b (black points). Band gaps are accepted to be small energies (between 3.06 and 3.25 eV) on the grounds of band gap value of ZnO on literature, which is 3.2 eV. 30 nm film, which was chosen as base for following experiments had bang gap energy of 3.14 eV. For all films, band gap was increasing with increasing thickness. This was reasoned to release of stress with increasing thickness, which was observed in XRD data (Figure 4.5). When stress was released, defect levels just above the valance band would be disappeared, which would lead to a small increase in band gap energy.

Reason of absorptions around 4 eV was not clear, but they would be related to excitations from lower levels of valance band to conduction band (Dekkers 2007).

4.2. Effect of Al Content

In order to obtain more conducting films, ZnO was extrinsically doped with Al atoms. The films were codeposited from separate ZnO and Al targets. ZnO target was sourced by an RF power source while Al was sourced by a DC power source. Deposition took place at room temperature and the temperature of substrates remained the same during the process. Deposition time of all the structures was 30 min and

working pressure was 3 mTorr. Substrates were rotated with a speed of 70 rpm. Ar gas is used in all depositions.

In the first place, Al content of the films was varied by changing deposition power of Al. ZnO was deposited at a fixed power of 60 W, whereas Al power was varied at 20, 10, 5 and 2.5. Al thickness was estimated from growth rate by timing and content of the films was assumed as the ratio of Al thickness to total thickness of the films. Increasing Al deposition power increased growth rate, leading to higher Al content. Deposition power, thickness, roughness and calculated Al content of Al doped ZnO films are presented in Table 4.2.

Table 4.2. Deposition power, thickness and calculated Al content of Al doped ZnO films.

Al Power (W) (DC)	Thickness (nm)	Calculated Al Content (%)
0 W (Pure ZnO)	30	0
20 W	60	50
10 W	54	46
5 W	51	43
2,5 W	40	27

4.2.1. XRD Results

XRD scans of films with various Al contents are given in Figure 4.12. Scan of pure ZnO with similar thickness is given for comparison. It was observed that ZnO (002) peak diminished more with Al introduction into the films indicating that crystal structure was degraded. This inferred that Al atoms did not replace with Zn atoms substitutionally, instead they accumulated on interstitial sites, preventing crystallization of ZnO. When deposition power of Al was 20 W (corresponding to content of about 50%), two new peaks corresponding to metallic Zn in (101) and (100) directions occurred. According to peak chart of Zn, it is known that Zn (101) is the most intense peak for hexagonal phase, therefore, Zn in the film was in hexagonal phase, similar with pure ZnO films. This implied that O atoms in ZnO structure were removed and

hexagonal ZnO structure turned into hexagonal metallic Zn. Oxygen atoms were predicted to oxidize Al atoms in the structure, causing Al to turn into AlO_x in amorphous phase.

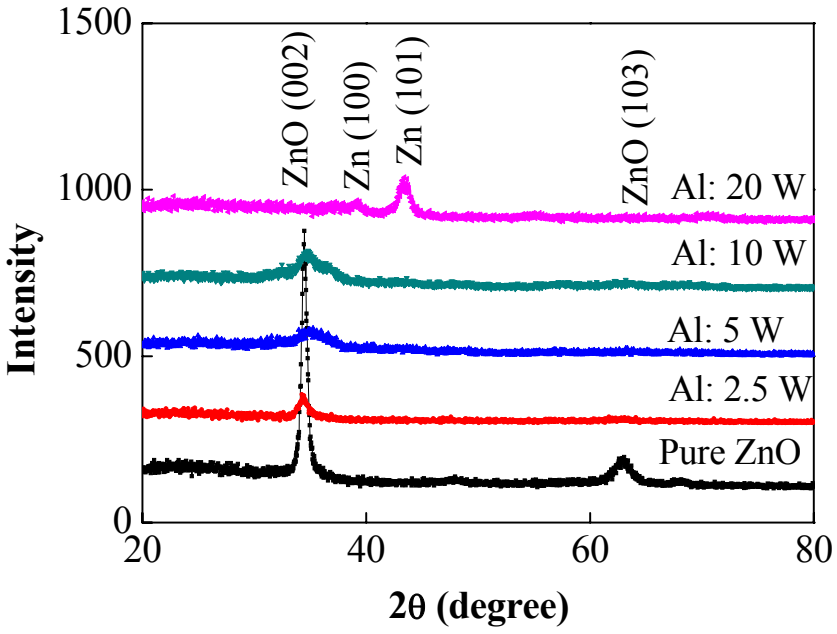

Figure 4.12. XRD patterns of Al doped ZnO films with various Al contents.

4.2.2. SEM Results

As mentioned above, SEM images of pure ZnO films showed granular structure. However, in Al introduced films, grains were observed on the surface as shown on Figure 4.13. Surface images of films in which Al deposition powers were 20 and 5 W respectively, are shown in Figure 4.14 with 500 and 200 scales. 500 nm scaled image does not show significant difference on the surfaces for 20 and 5 W Al deposition power. In 200 nm scale, it was observed that 20 W film had larger grains than 5 W film. These images implied that grains on the surface were originated from Al. Because pure ZnO films did not have grains and film with higher Al content had bigger grains.

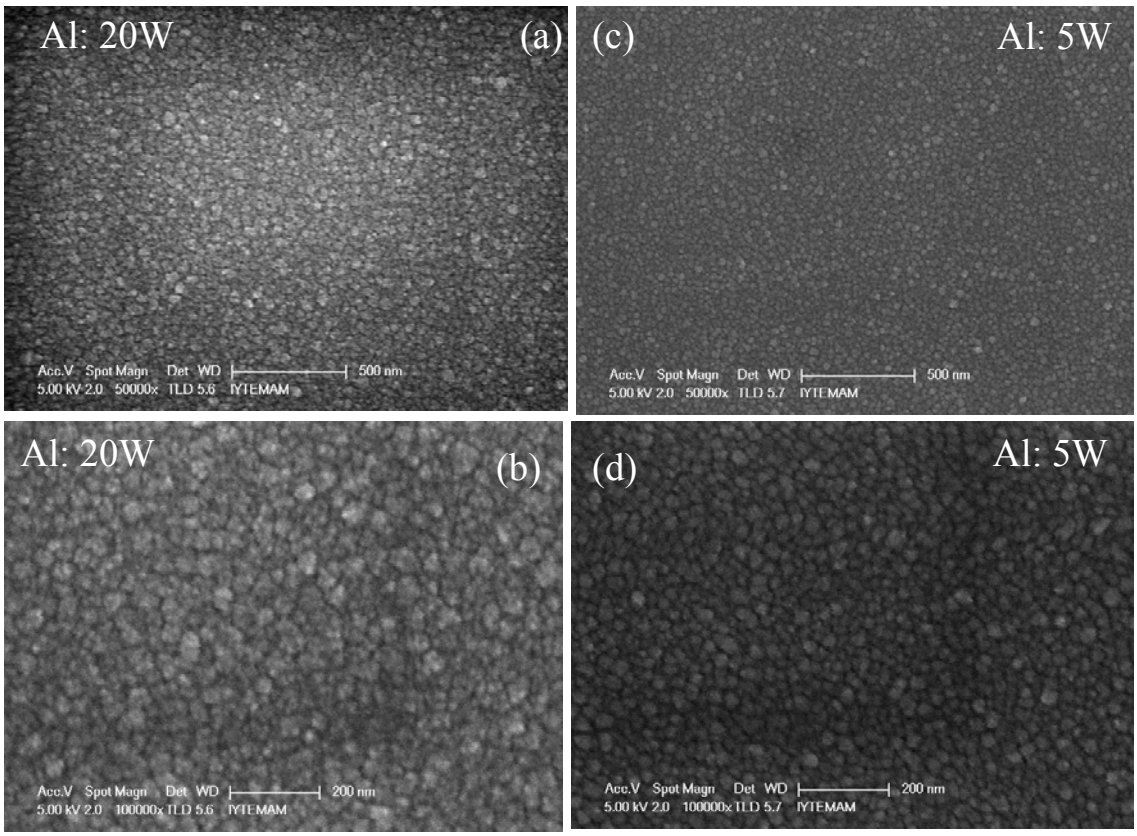

Figure 4.13. SEM images of Al dopped films with Al deposition power of (a), (b) 20 W and (c), (d) 5 W. (a) and (b) have 500nm scales while (c) and (d) have 200 nm scales

4.2.3. Resistivity Results

Sheet resistance was obtained with the help of four point probe technique. Four point probe technique is a conventional technique that enables to obtain true lateral resistance (sheet resistance) by eliminating resistance of the contacts and wires.

Resistivity was calculated by using sheet resistance and thickness values according to the formula:

$$\rho = R_S.t = 4.53\, R\, t \tag{4.9}$$

where R_S is the sheet resistance, t is the thickness, 4.53 is the correction factor for square shaped samples and R is the resistance obtained from the four point probe measurement.

Figure 4.14 shows the relationship between Al content and resistivity of uniformly doped samples.

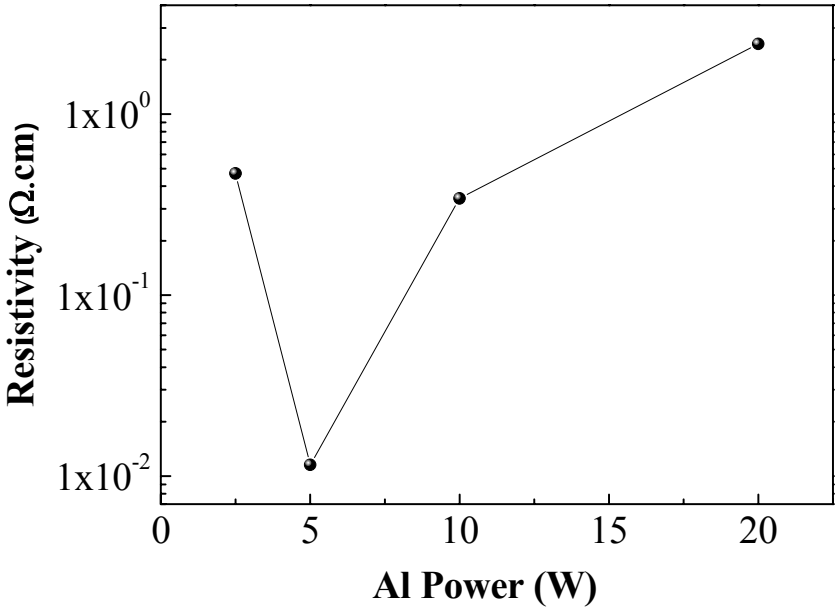

Figure 4.14. Resistivity values of Al doped ZnO films with various Al contents.

It was observed that resistivity decreased rapidly from 2.44 Ωcm to the minimum value of $1.5x10^{-2}$ Ωcm when deposition power of Al was decreased from 20 to 5 W (calculated content was decreased from 50% to 43%). However, when Al deposition power was further decreased to 2.5 W, resistivity increased to $4.7x10^{-1}$ Ωcm. According to transmission data, when doping was performed with 2.5 W, transmission of the film was very close to that of pure ZnOs. This implied that deposition of Al may be less effective than expected. This was probably because 2.5 W was not enough to create Al atoms energetic enough to reach and adhere on the film surface.

The observation of higher resistivity for deposition powers higher than 5 W might be attributed to grain boundary scattering. Because XRD results showed that crystal structure of the films degraded and films turned into amorphous. It can be seen on the literature as well that carrier transport is limited by grain boundary scattering due to charged defects at grain boundaries (Ellmer and Vollweiler 2006). Other scattering mechanisms such as impurity clustering and ionized impurity scattering may also have contributed to the increase of resistivity (Ellmer and Vollweiler 2006). It is known that as impurity content increases, impurity atoms coalesce together and form clusters which

cause free electrons to be scattered. High impurity concentration leads to positively charged ionized impurity centers making free electrons scatter as a result of coulomb interaction between impurity centers and free electrons.

To sum up the effect of Al deposition power; minimum resistivity of 1.15×10^{-2} Ωcm was achieved with deposition power of 5 W (calculated content was roughly 43%). Therefore, in the following films, 5 W is used as deposition power for Al.

4.2.4. Transmission Results

Transmission spectra of Al doped ZnO films is given in Figure 4.15. Bare glass and pure ZnO spectra was inserted on the graph as reference. It was seen that transmission of pure ZnO and Al doped ZnO with lowest Al power (2.5 W) was almost the same. Therefore it could be concluded that Al did not grow significantly. Also the shoulder observed in pure ZnO spectrum at about 400 nm disappeared when Al was introduced. When deposition power of Al was decreased to 5W, transmission decreased to the half value of pure ZnO and decreased further as deposition power of Al was further decreased.

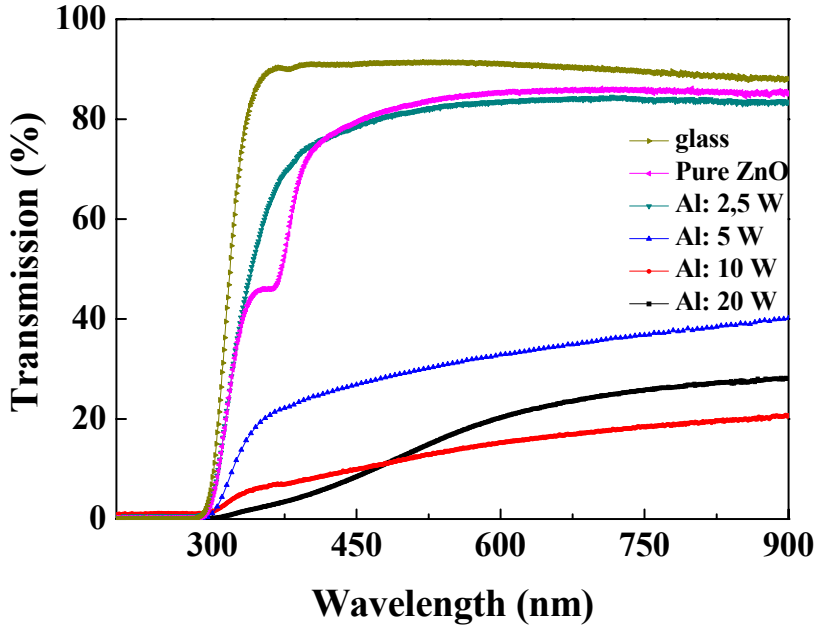

Figure 4.15. Transmission spectra of Al doped ZnO films with various Al contents.

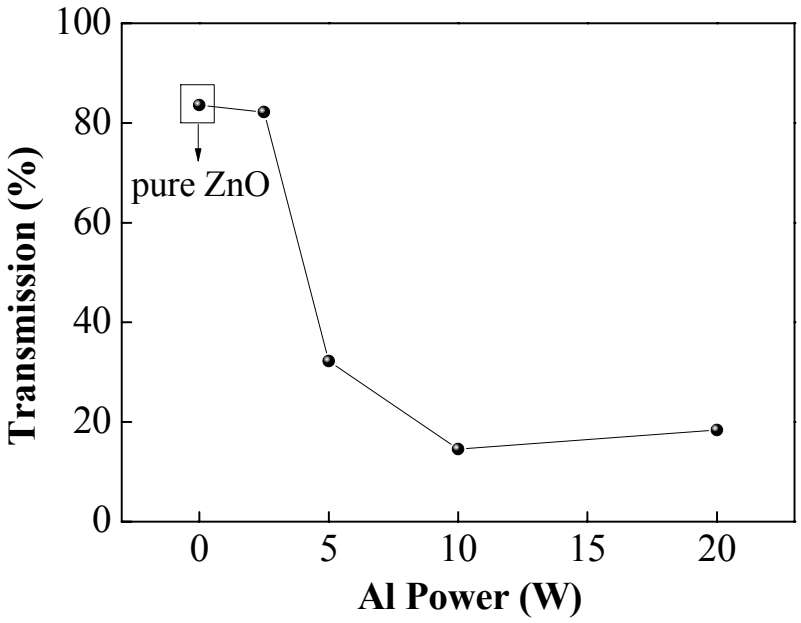

Figure 4.16. Average transmission between 400-800 nm of Al doped ZnO films.

Average transmission values of doped films between 400-800 nm are shown in Figure 4.16. Rapid drop in transmission starting from 5 W might be attributed to high dopant concentration as free electrons reflected the light and caused decrease in transmission (Robbins and Wolden 2003).

Band gap energy of Al doped ZnO films can be found by extrapolating α^2 vs $h\nu$ graph. However, it is very critical to emphasize that for low transmission values, reflections can not be ignored. Therefore, such low transmissions prevent an accurate calculation of the optical gap by extrapolation method (Dekkers 2007). The calculated band gap values for Al doped films are given in Figure 4.17.

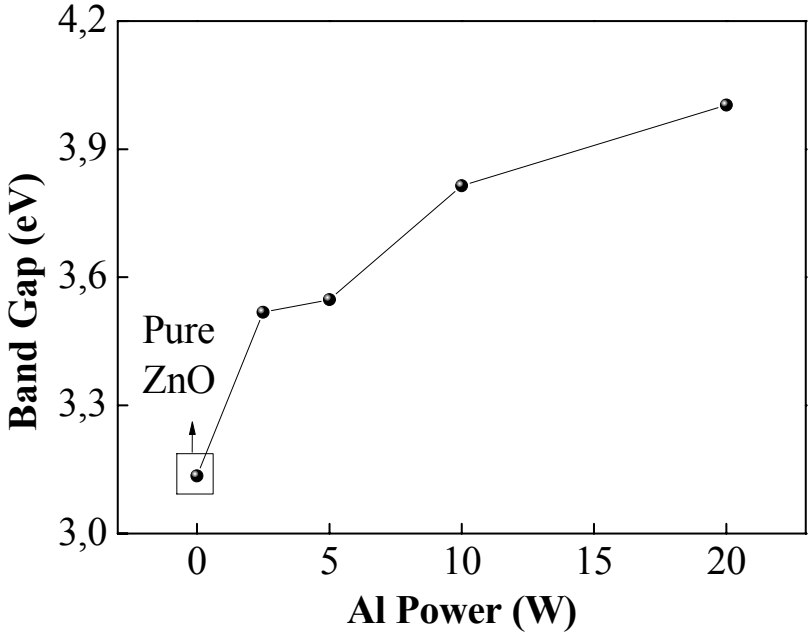

Figure 4.17. Band gap values of Al doped ZnO films.

To summarize the effect of Al content, it was seen that high contents destroyed crystal structure and resulted in amorphous films. ZnO:Al films doped with higher Al deposition power (hence higher Al concentration) were poor in transmission. Band gaps of highly doped films were larger as well. Resistivity of highly doped films was higher, which was in correspondence with larger band gap values. Lower values of resistivities were obtained with lower contents of Al. The lowest resistivity obtained was 1.15×10^{-2} Ωcm and transmission corresponding to the film was 8.3% and was very poor. Therefore content of Al must be decreased further in order to obtain higher transparent films.

4.3. Effect of Modulation Doping

It is known that increasing number of ionized impurities decreases mobility hence decreases conductivity. Since amount of ionized impurities are related to dopant concentration, in order to obtain more conductive and transparent films, doping concentration (Al content) would be decreased. Therefore, for our case, Al doping concentration must be decreased further. However, decreasing the content by lowering

deposition power of Al was not possible because as it was discussed in the previous section. Decreasing power below 5 W resulted in unstable plasma and ineffective Al growth.

To decrease the Al content of the films and increase the transmission, a method named “modulation doping” was employed (details were given in Chapter 3).

In modulation doping, heavily doped and undoped thin layers are stacked on top of each other. Carriers from heavily doped region segregate into undoped region as a result of a potential originated from band gap difference of layers. Ionized impurities that are left behind by the migrating carriers are remained in heavily doped region. Since carriers are transported in relatively ionized impurity free region, mobility increases and resistivity decreases.

We performed modulation doping by means of depositing periodic stacks of pure ZnO and Al doped ZnO. Pure ZnO layers corresponded to transport layers whereas Al doped ZnO layers corresponded to doping layer.

The deposition procedure can be summarized as follows: power of Al was fixed to 5 W and stacks of pure ZnO and Al doped ZnO were deposited periodically. This lead to stacks of pure ZnO (as transport layer) and ZnO:Al layers (as doping layer) with fixed Al content. Total deposition time of films was fixed to 30 min for all films. Also, in individual films, total thicknesses of stacks were kept constant. For different films, only the thickness of pure ZnO layers was increased. In this way, while content of individual ZnO:Al layers was fixed, total content of films was decreased. Structure of the films is illustrated in Figure 4.18.

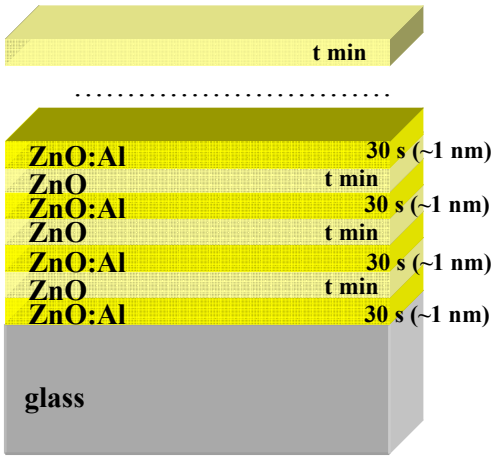

Figure 4.18. Illustration of modulation doped films. Thickness of ZnO layers were fixed while thickness of ZnO:Al layers were varied by timing.

Thicknesses of layers were estimated by deposition time. Thickness of doping layer was fixed to ~1 nm (30 s) whereas thickness of transport layer was varied as ~0.5 nm (30 s), ~1nm (60 s), ~1.5 nm (90 s), ~2 nm (120 s) and ~3 (180 s) nm, referring the work of Robbins and Wolden (2003). (They concluded that the layer thicknesses of transport and doping layers must be under ~5 nm in order to benefit from this method.) The method gave the chance of decreasing Al content and increasing the mobility of the films at the same time.

Pure ZnO layer (transport layer) thickness, total thickness and corresponding Al content of films are given in Table 4.3. As mentioned before, thickness values were adjusted by timing the growth.

Table 4.3. Pure ZnO layer (transport layer) thickness, total thickness and corresponding Al content of films.

Pure ZnO Layer Thickness (nm)	**Total thickness (nm)**	**Al Content (%)**
0 nm (Uniformly doped film)	~51 nm	~43%
~0,5 nm (30 s)	~40 nm	~25%
~1 nm (60 s)	~37 nm	~19%
~1,5 nm (90 s)	~35 nm	~14%
~2 nm (120 s)	~34 nm	~12%
~3 nm (180 s)	~33 nm	~8%
30 nm (30 min) (Pure ZnO film)	~30 nm	0

4.3.1. XRD Results

Figure 4.19 shows XRD pattern for films with varying transport layer thicknesses (pure ZnO thickness). Patterns for 30 nm pure ZnO and uniformly Al doped ZnO with the lowest resistivity are given to make a comparison.

As mentioned in previous part, crystal structure of Al doped films degraded and all peaks vanished from the spectrum. When modulation doping applied, it was observed that ZnO crystal structure reappeared. As thickness of pure ZnO layer increased, ZnO (002) peak became more significant, indicating that ZnO layers between

doped layers crystallized preferentially in (002) direction similar with pure ZnO. Also growth in (103) direction was observed as transport layer thickness was increased. It can be seen on the spectrum that crystal structure of pure ZnO and the films with 3 nm ZnO layers were very close to each other. This implied growing Al containing films with almost the same crystal quality as pure ZnO was possible.

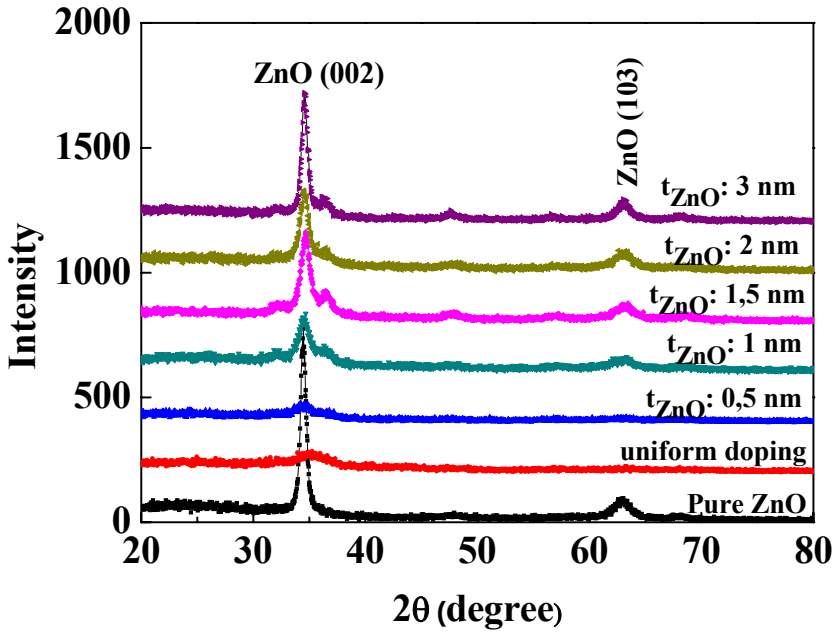

Figure 4.19. XRD pattern for films with varying transport layer thicknesses.

Figure 4.20 shows grain size values of films calculated with Scherer formula. As mentioned before, uniformly doped films were almost. When instead of uniform doping, modulation doping was applied, grain size of ZnO crystals between doped layers increased with increasing pure ZnO layer thickness. It was seen that grain size increased from 10 nm to 15.5 nm when pure ZnO layer thickness increased from ~0.5 nm to ~3 nm. Grain size of the film with ~3 nm transport layer was very close to that of pure ZnO film (30 nm).

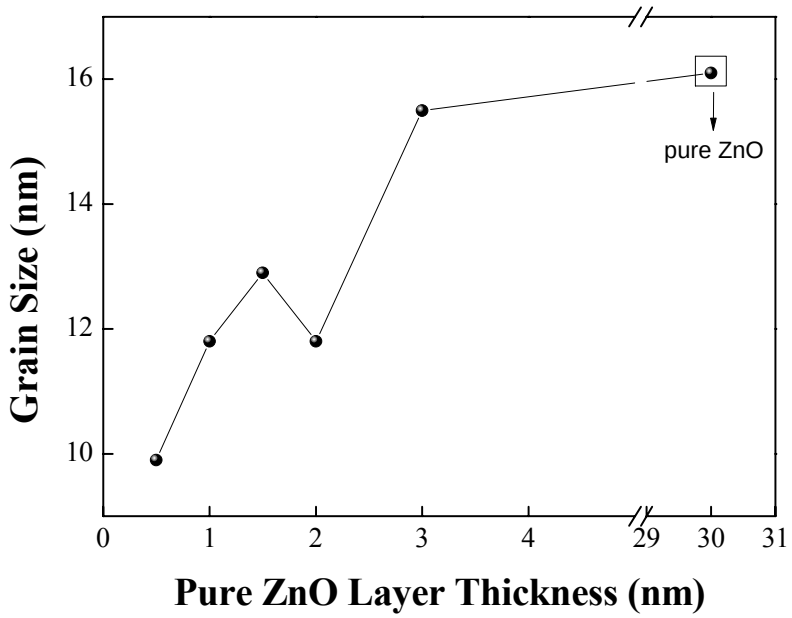

Figure 4.20. (a) Grain sizes of ZnO (002) peaks of modulation dopped films.

4.3.2. SEM Results

SEM pictures with 200 nm scale of the surface of modulation doped films are shown in Figure 4.21. Similar to uniformly doped films, modulation doped films showed grainy structure. There was no significant change on the surface and grain sizes were close in both cases.

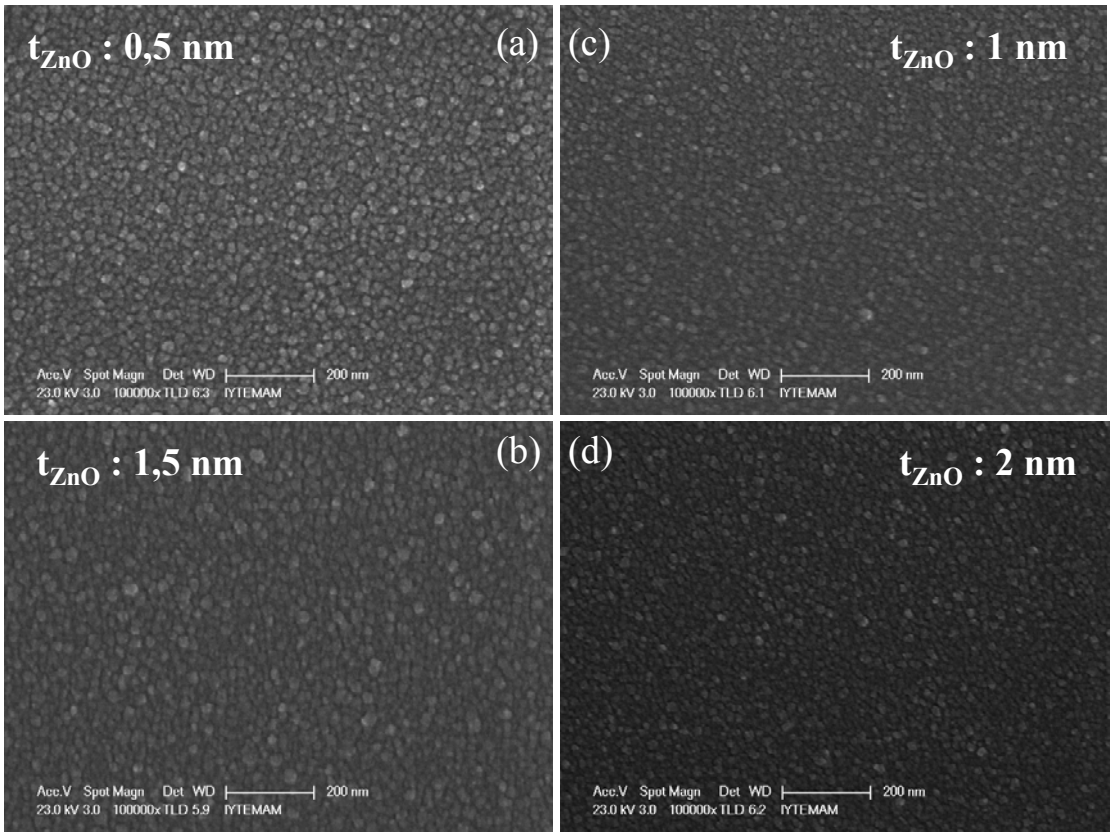

Figure 4.21. SEM images of modulation doped films.

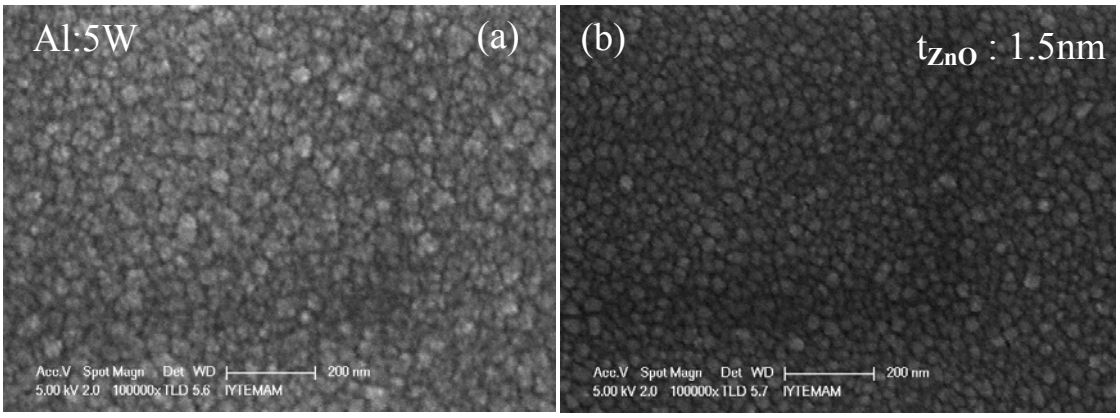

Figure 4.22. SEM images of (a) uniformly doped and (b) modulation doped (pure ZnO layer thickness: 1,5 nm).

SEM images of uniformly doped and modulation doped films with 1.5 nm pure ZnO layer thicknesses are compared in Figure 4.22. Films with 1.5 nm thick pure ZnO layers were chosen because they had the lowest resistivity amongst modulation doped films. It was seen that, grain size of modulation doped film was smaller. This might be attributed to decrease of Al content owing to decrease in time of Al deposition.

4.3.3. Resistivity

As mentioned before, in our case, heavily Al doped ZnO (ZnO:Al) layers were doping layers that act as carrier source and pure ZnO layers were transport layers.

Resistivity values of the modulation doped films with different transport layer thicknesses are shown in Figure 4.23. Resistivity of uniformly doped film of 30 nm is given as reference.

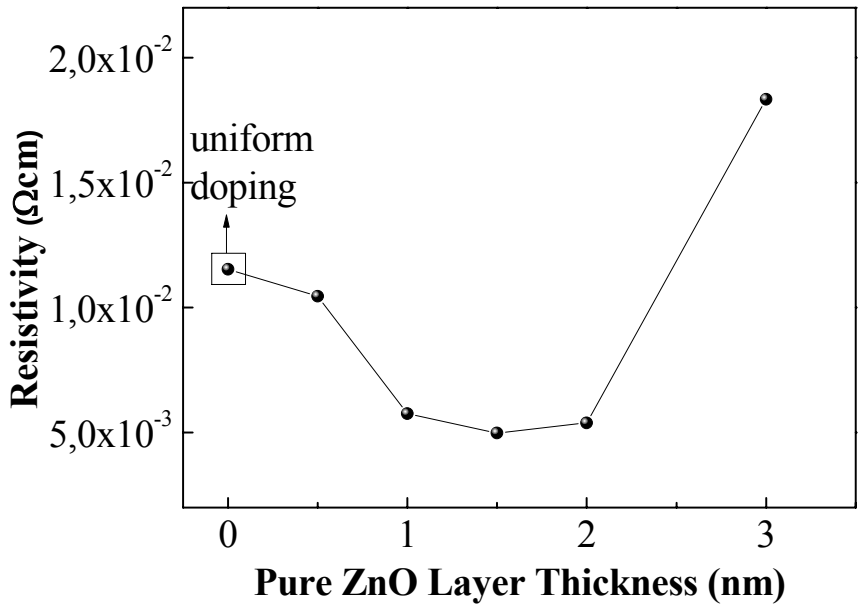

Figure 4.23. Resistivity of films with various transport layer (ZnO) thickness.

It was observed that resistivities of films were decreasing as thickness of transport layer was increasing until thickness of ~1.5 nm. For ~2 nm it remained almost the same, and than increased suddenly for ~3 nm. Decrease in resistivity could be related to increase of mobility owing to layered structure (Ellmer and Vollweiler 2006, Dingle, et al. 1978, Rauf 1993, Robbins and Wolden 2003). If it was assumed that Al diffusion was negligible during the room temperature growth, each ZnO layer would contain only unintentional background impurities. Electrons from dopant layer might have segregated from ZnO:Al layers to ZnO layers. Since carrier concentration was less in ZnO layers, electrons could transport with higher mobility compared to uniformly doped structures owing to elimination of ionized impurity scattering.

Decreasing resistivity could also be attributed to reappearance of crystallization in (002) direction for pure ZnO layers. Crystallization by the help of modulation doping would reduce grain boundary scattering in transport layer. By layered growth, total amount of Al in the films changed although content of the Al doped layers were fixed. Owing to decrease in carrier concentration, impurity clustering might have been decreased as well. This would lead to increase of mobility and decrease in resistivity as reported previously (Ellmer and Vollweiler 2006, Dingle, et al. 1978, Rauf 1993, Robbins and Wolden 2003).

To summarize, the lowest resistivity of 4.98×10^{-3} Ωcm was obtained with transport layer thickness of 1,5 nm (Al content: about 14%). This result was consistent with the prediction of (Ellmer 2001) claiming that resistivity of modulation-doped layers would be limited to 1.5×10^{-3} Ωcm (since the transferred maximum electron sheet density is only about 10^{13} cm^{-2}).

4.3.4. Transmission

Transmission spectra of modulation doped films were given in Figure 4.24. Spectra of bare glass and uniformly doped ZnO films were given as reference.

As can be seen in Figure 4.25, when modulation doping was applied, average transmission of uniformly doped film increased from 38% to 48%. Transmission increased linearly with increasing thickness of pure ZnO layer and got closer to the transmission value of pure ZnO. This result would be attributed to decease of total Al concentration. Highest transmission of 74% was observed in films with 3 nm pure ZnO layers. Transmission of the film with the lowest resistivity (pure ZnO layer thickness was 1.5 nm) was 69 %.

It was also observed that similar with uniformly doped films, except the film with 3 nm ZnO layers, did not have the shoulder at about 350 nm in the transmission data. In the 3 nm layered the shoulder appeared and its spectrum was similar to pure spectrum of ZnO films. Indeed, amongst modulation doped films, highest transmission of 74% was observed in this film.

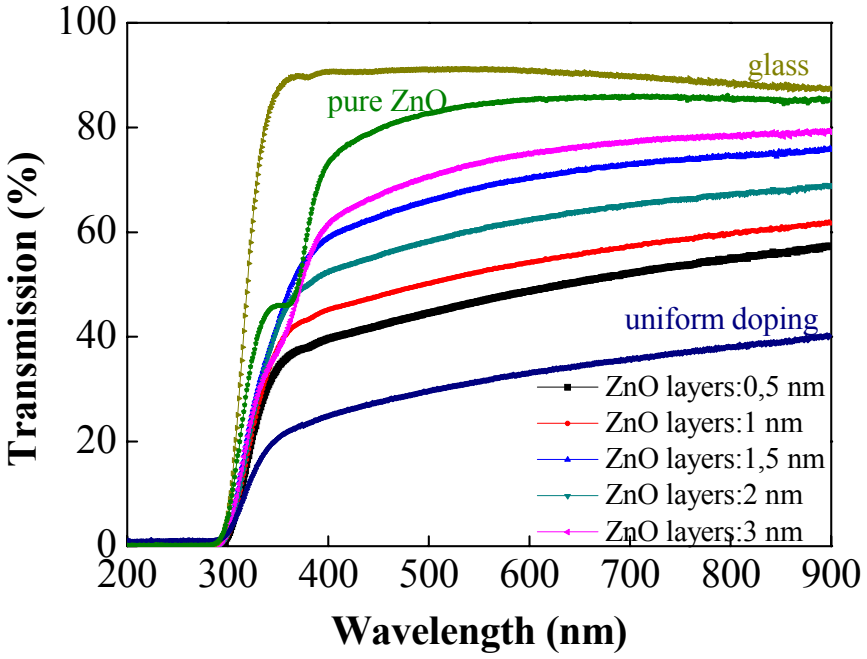

Figure 4.24. Transmission spectra of modulation doped films.

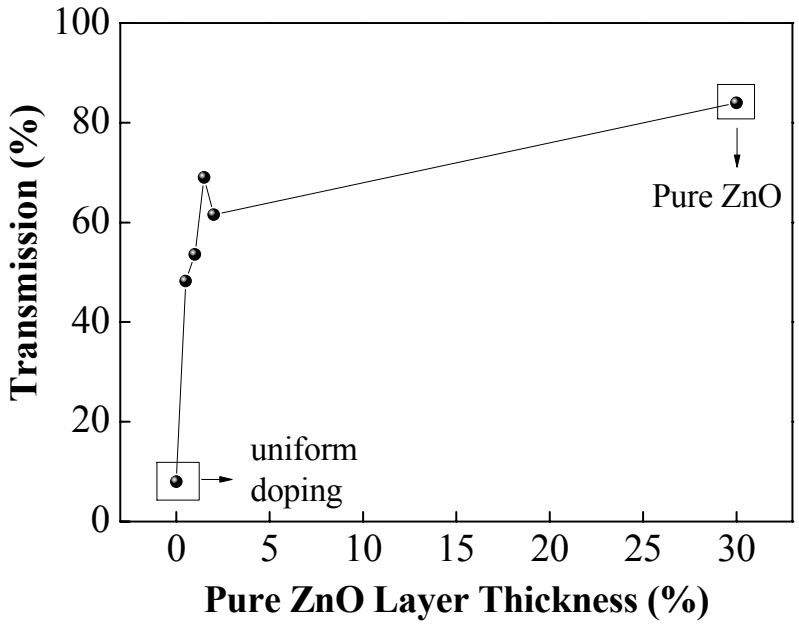

Figure 4.25. Average transmission between wavelengths 400-800 nm of modulation doped films.

Figure 4.26 shows band gap determination plot for modulation doped films. Inset of the plot shows a closer look to 3 nm layered film second absorption, which is

similar to the case of pure ZnO. Band gaps of values of modulation doped films are given in Figure 4.27. It was seen that modulation doped films had wider band gaps than uniformly doped films. Band gap values of films with ~0.5, ~1, ~1.5, ~2 nm films were in the range between 4.04 eV and 4.09 eV. ~3 nm layered film showed two band gaps which are 3.14 eV and 4.06 eV, which was similar with the case of pure ZnO. It was also seen in XRD results that the film with 3 nm pure ZnO layer had almost the same crystal structure with pure ZnO films. Therefore 3.14 eV was reasoned to pure ZnO layers. Widening of band gap for these films can be attributed to prevention of band gap narrowing. It is known that once the material becomes degenerate, columbic interactions shift the conduction band downwards and the valence band upwards and effectively narrows the band gap (Franken 2006, Bashar 1998). For our case, decrease of Al content may have led to non-degenerate films, therefore increased the band gap.

Crystal and band structure of modulation doped film with ~3 nm pure ZnO layer was similar to that of pure ZnO as mentioned. However, resistivity of pure ZnO was out of the device range, while resistivity of modulation doped film was 4.17×10^{-3} Ωcm. Therefore we can conclude that it is possible to fabricate more conducting films with almost the same band gap and crystal structure as pure ZnO.

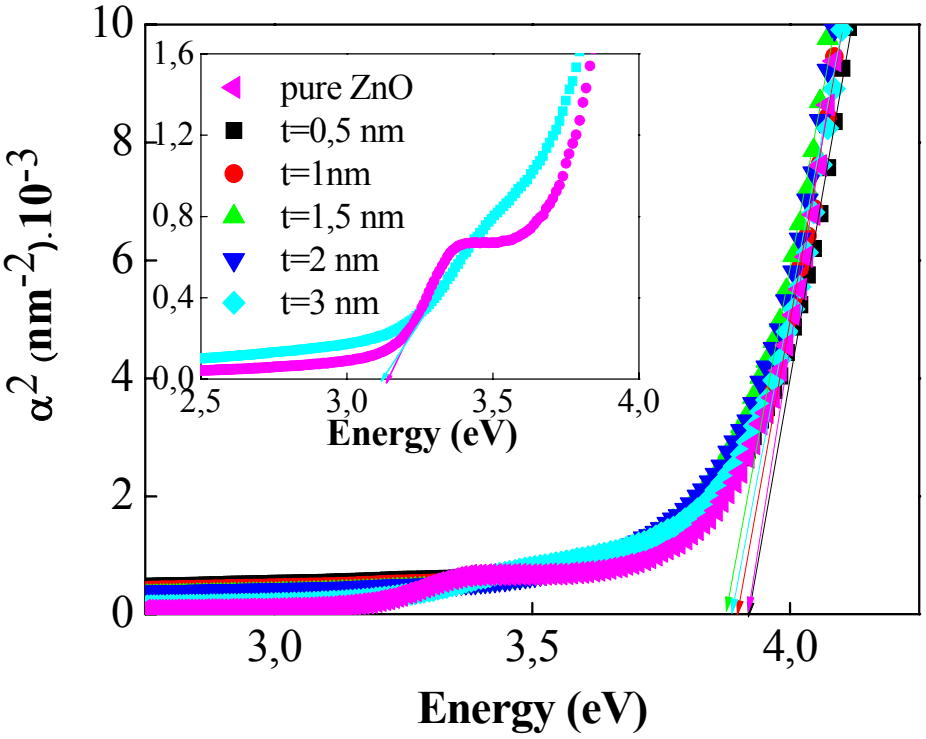

Figure 4.26. Square of absorption coefficient vs photon energy plot for band gap energy calculation of modulation doped films.

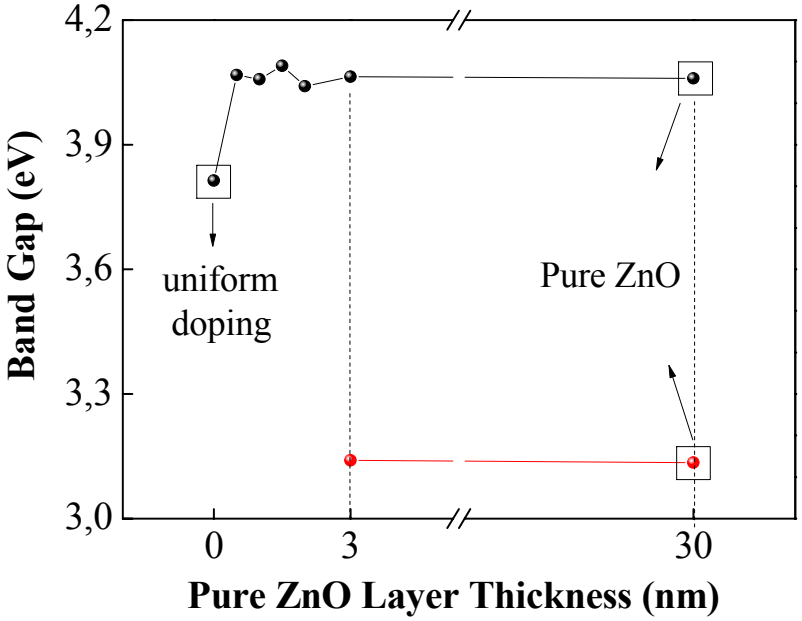

Figure 4.27. Band gap energy of modulation doped films.

4.4. Effect of Substrate Bias

In order to improve conductivity and transmittance of films, we also used a method inspired from the work of Lee and Song (2008). In their study, they applied dc bias voltage to the substrates during deposition. Different from them, we applied rf bias voltage due to the rf source (with a maximum power of 50W) connected to the substrate holder of our system.

We redeposited modulation doped film with the lowest resistivity (4.98×10^{-3} Ωcm) by applying various rf bias voltages to substrate holder during deposition. Applied rf bias voltages were 5, 10, 20W. When bias applied, Ar gas in the environment discharged and Ar plasma occurred. This meant that during deposition, besides ZnO and Al plasma, additional Ar plasma existed in the chamber. Therefore during growth, films were being back sputtered at the same time. The process was equivalent to a combination of simultaneous deposition and backsputering (etching) of films.

Growth took place at room temperature at a working pressure of 3 mTorr and samples were rotated with a speed of 70 rpm. Other deposition parameters are given in Table 4.4.

Table 4.4. Deposition parameters for growth of biased samples.

Deposition and Bias Parameters	
Working Pressure	3 mTorr
Al power	5 W (DC)
ZnO power	60 W (RF)
Growth Temperature	25^0C
Applied Bias Power	5 W, 10W,20W (RF)

4.4.1. XRD Results

In Figure 4.28, XRD patterns of biased samples are shown. For comparison, the pattern of the film deposited with the same parameters without bias is also given. For 5

W bias, (002) peak shifted to small angle side and calculated strain was 1.485%. This suggested that Al^{+3} ions were located on interstitial sites. If they were substitute for Zn^{+2} ions, the lattice would be compressed due to smaller radius of Al compared to Zn^{+2}. When lattice was compressed, (002) peak would shift to higher diffraction angle (Chung, et al. 2006).

It was seen that (002) and (103) peaks vanished with increasing bias power, while (101) and (110) peaks were becoming more dominant. This implied that crystal structure deteriorated with bias application and preferred orientation was changing from (002) to (101) direction. This result was the opposite results in literature, which claims bias application up to 40 V improves crystallinity (Lee and Song 2008).

Degrading of crystal structure can be attributed to a few possibilities. One possibility is back sputtering of atoms which may be associated with etching of film from the surface because of additional Ar plasma. If back sputtering (etching) rate was larger than sputtering rate, ZnO might not have grown thick enough to exhibit crystal structure. Apart from this, Ar ions and electrons of the additional plasma might result in scattering of sputtered species before they reach the substrate and prevent them sticking onto the substrate to form a film.

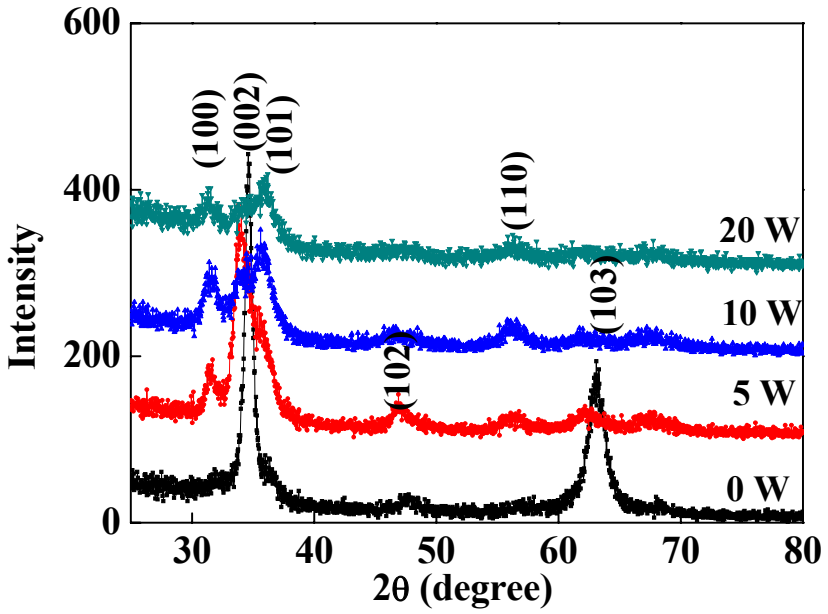

Figure 4.28. XRD patterns of biased samples.

4.4.2. SEM Results

Figure 4.29 shows surface of modulation doped films deposited without substrate bias and with 10 W substrate bias. Both of the films were modulation doped with 30 s grown (~1.5 nm) transport layer. Film on Figure 4.29.a. was deposited without bias and the one on Figure 4.29.b. was deposited with 10 W bias. The film grown with no bias had the lowest resistivity of undoped films, and 10 W biased films had the lowest resistivity of biased films. 10 W biased film was seemed to be smoother than unbiased film.

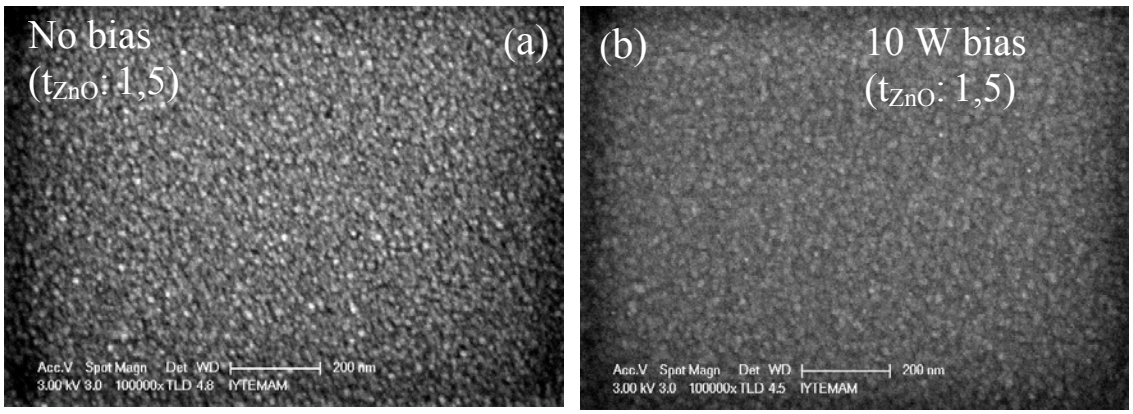

Figure 4.29. SEM images of films deposited (a) without substrate bias and (b)with 10 W substrate bias.

4.4.3. Resistivity

As can be seen on Figure 4.30, Resistivities of the samples decreased for bias powers of 5W and 10W. However, when 20 W was applied, resistivity exceeded the resistivity of non biased sample. The lowest resistivity of 2.03×10^{-3} Ωcm was achieved with 10 W bias. Unlike work of (Lee and Song 2008), decrease in resistivity could not be explained with improvement of crystal structure due to bias application since XRD data showed that crystal structure degraded when bias voltage was applied. An explanation to decrease in resistivity might be decrease of Al content to more convenient limits as a result of decreasing deposition rate. Collisions between sputtered Al atoms and Ar ions and electrons of additional Ar plasma may have decreased the

growth rate of Al. Decrease in resistivity might also be related to improvement of interface between pure ZnO and ZnO:Al layers. Ions and electrons of additional Ar plasma might have removed loosely bounded atoms from the surface, in other words, polished the surface and led to smoother interfaces. Smoother interface means less scattering at the interfaces and easier transport for carriers to reach to transport layer. By this way, mobility would be higher leading to lower resistivity.

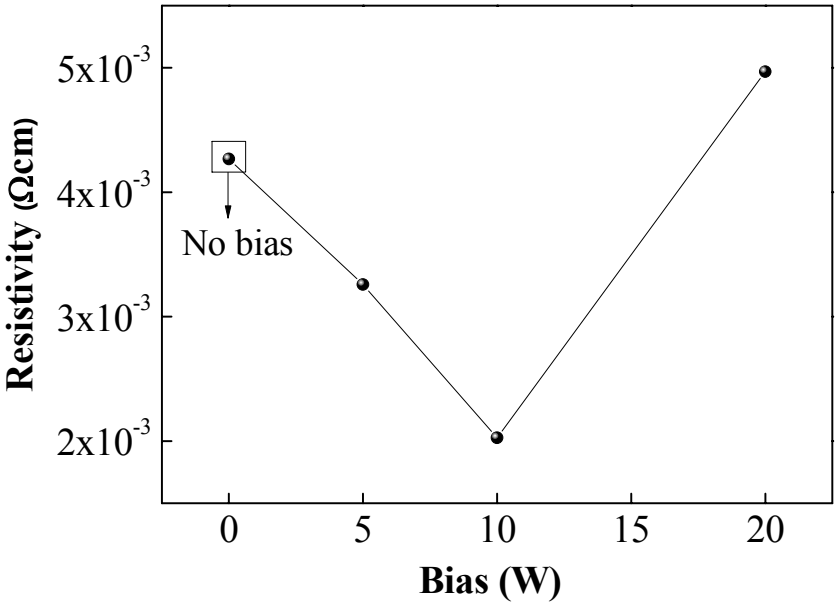

Figure 4.30. Resistivity vs applied bias power.

4.4.4. Transmission

Figure 4.31 and 4.32 shows transmission spectra and average transmission values between wavelengths 400-800 nm. Pure ZnO and film grown without bias is given for comparison. It was seen that bias with 5 W and 10 W increased transmittance from 69% to 78% and 79%, respectively. When bias was increased to 20 W, the transmittance of the films was seen to approach to pure ZnO transmittance. This might be attributed to decrease in total thickness of the films owing to decrease in deposition rates of ZnO and Al.

From XRD data it was observed that ZnO peaks vanished with increasing power. Assisted with transmission data, it was concluded that deposition rate for especially ZnO had substantially decreased. Al content might have been decreased as well because

otherwise transmission value of films would be higher, as was observed in films with higher Al concentrations. Increase of transmission might be attributed to decrease in total Al content, leading to fewer carriers, which might result in decrease of free carrier absorption (Cohen and Barnett 2005). Also if interfaces got smoother, this would have prevented scattering on the interfaces and increased transmission.

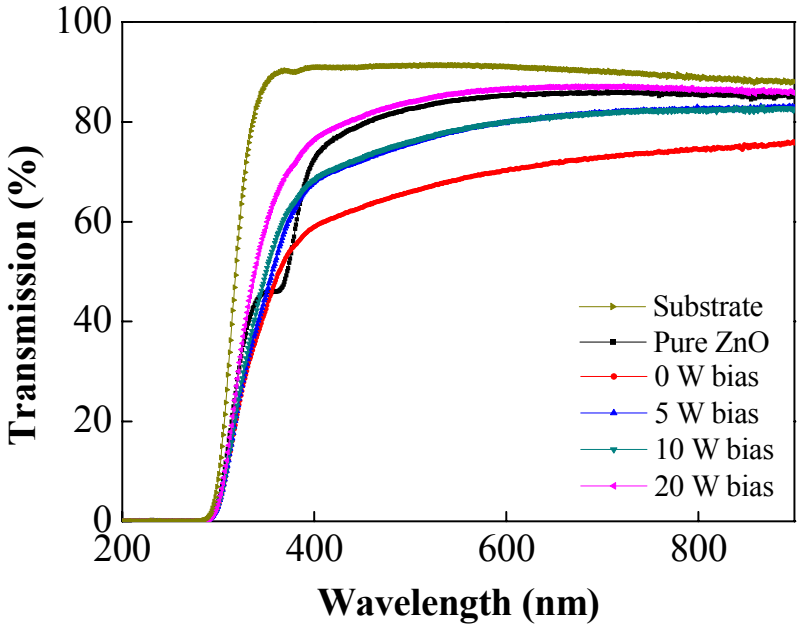

Figure 4.31. Transmission spectra of biased films.

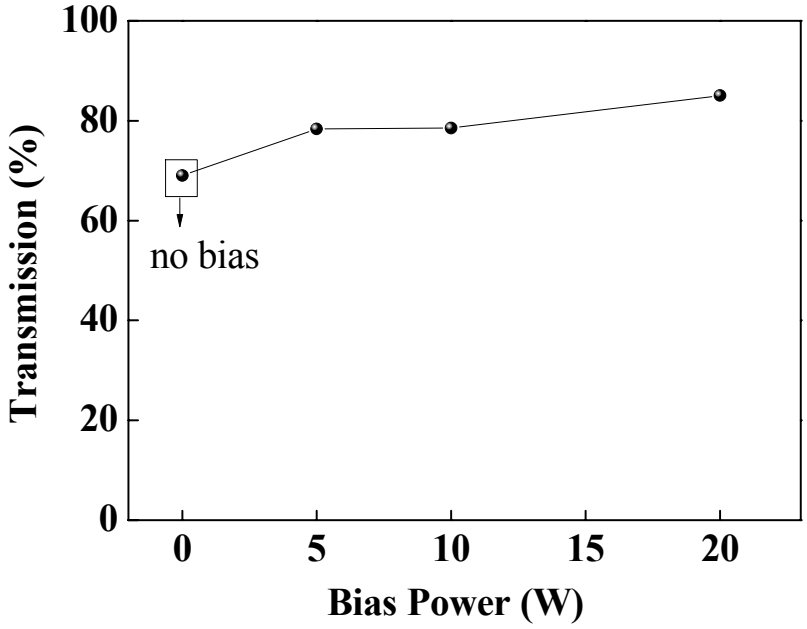

Figure 4.32. Average transmission of biased samples between 400-800 nm.

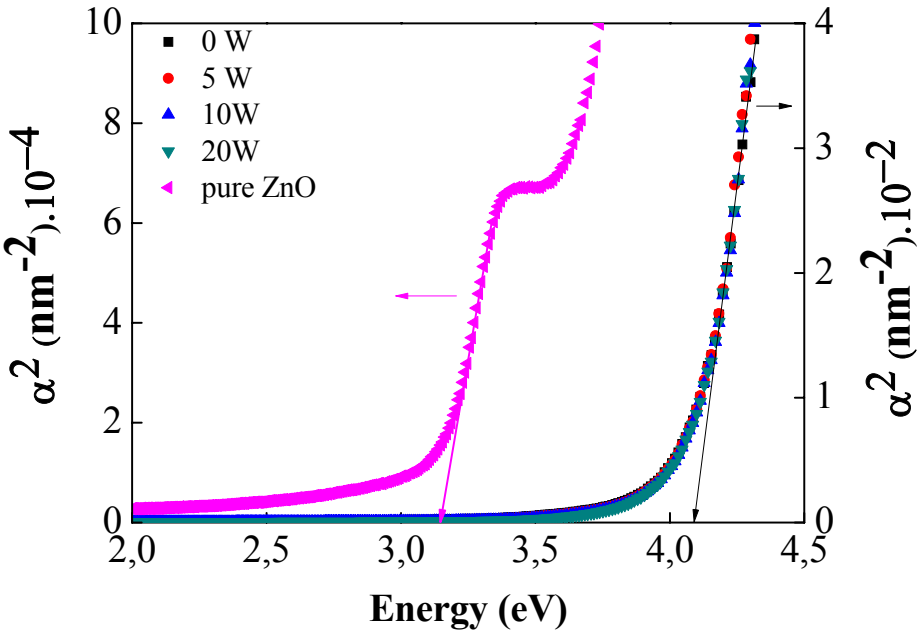

Figure 4.33. Extrapolation for defininition of band gaps of biased samples.

Band gaps of biased samples were defined by extrapolation of α^2 vs photon energy graph (Figure 4.33). Defined band gaps are shown in Figure 4.34. Similar to trend observed in transmission, band gap values of the films increased with increasing

bias power. Film deposited with 20 W bias powers exhibited the highest transmission value of 85% and its band gap was defined to be 4.13 eV. As mentioned before 10 W biased film had the lowest resistivity. Transmission and band gap of 10 W film was 78.5% and 4.11 eV respectively.

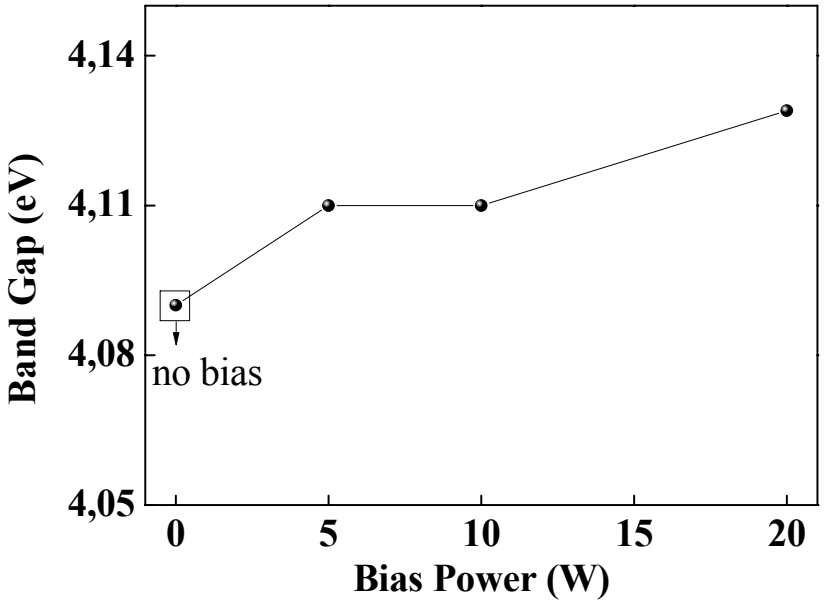

Figure 4.34. Band gaps of biased samples.

4.5. Annealing Effect

In order to improve optical and electrical properties of the films, post deposition annealing is applied. All samples were annealed at 300^{o}C for 1 hour in vacuum. Samples were rotated with a speed of 70 rpm. Before starting timing, we waited for 10 min for temperature stabilization. After annealing, samples were cooled to room temperature in vacuum.

Results that are given below belong to samples with the lowest resistivity of each set (pure ZnO, uniformly doped, modulation doped and biased samples). Each graph gives a comparison of non annealed and annealed result of corresponding parameters.

4.5.1. XRD Results for Annealed Samples

Figure 4.35 shows annealed and non annealed XRD spectrums of lowest resistivity samples of each set (pure ZnO, uniformly doped, modulation doped and biased samples).

Due to work of Ellmer, et al., it was expected that appropriate annealing process in ZnO:Al/ZnO layers would improve the crystal structure (2008). It was expected that more Al^{+3} ions would be drive into ZnO layer to substitute parts of Zn^{+2} sites or incorporate more Al atoms in the interstitial positions. However, improvement in crystal structure that would lead this conclusion was not observed (except for biased sample). It was seen on XRD spectrum that crystal structure of pure ZnO, uniform and modulation doped ZnO samples did not improve significantly, which implied that no recrystallization was occurred in those films. Only in biased sample, a slight improvement in ZnO (002) peak was observed.

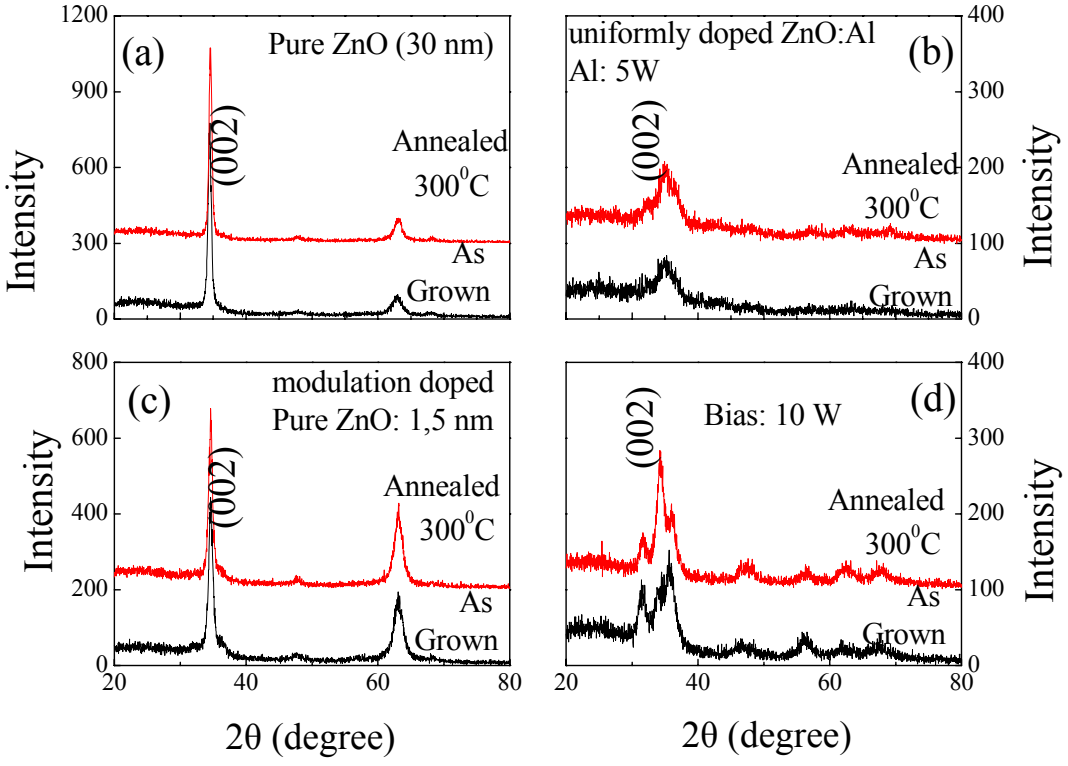

Figure 4.35. Annealed and as grown XRD spectrums of lowest resistivity samples of each set (a) pure ZnO, (b) uniformly doped; (c) modulation doped, and (d) biased samples.

4.5.2. SEM Results

Figure 4.36 shows a comparison of as grown and annealed uniformly doped ZnO films (lowest resistivity films of each set). Image of pure ZnO is not put because as mentioned in section 4.1.1.4, there were no grains on its surface.

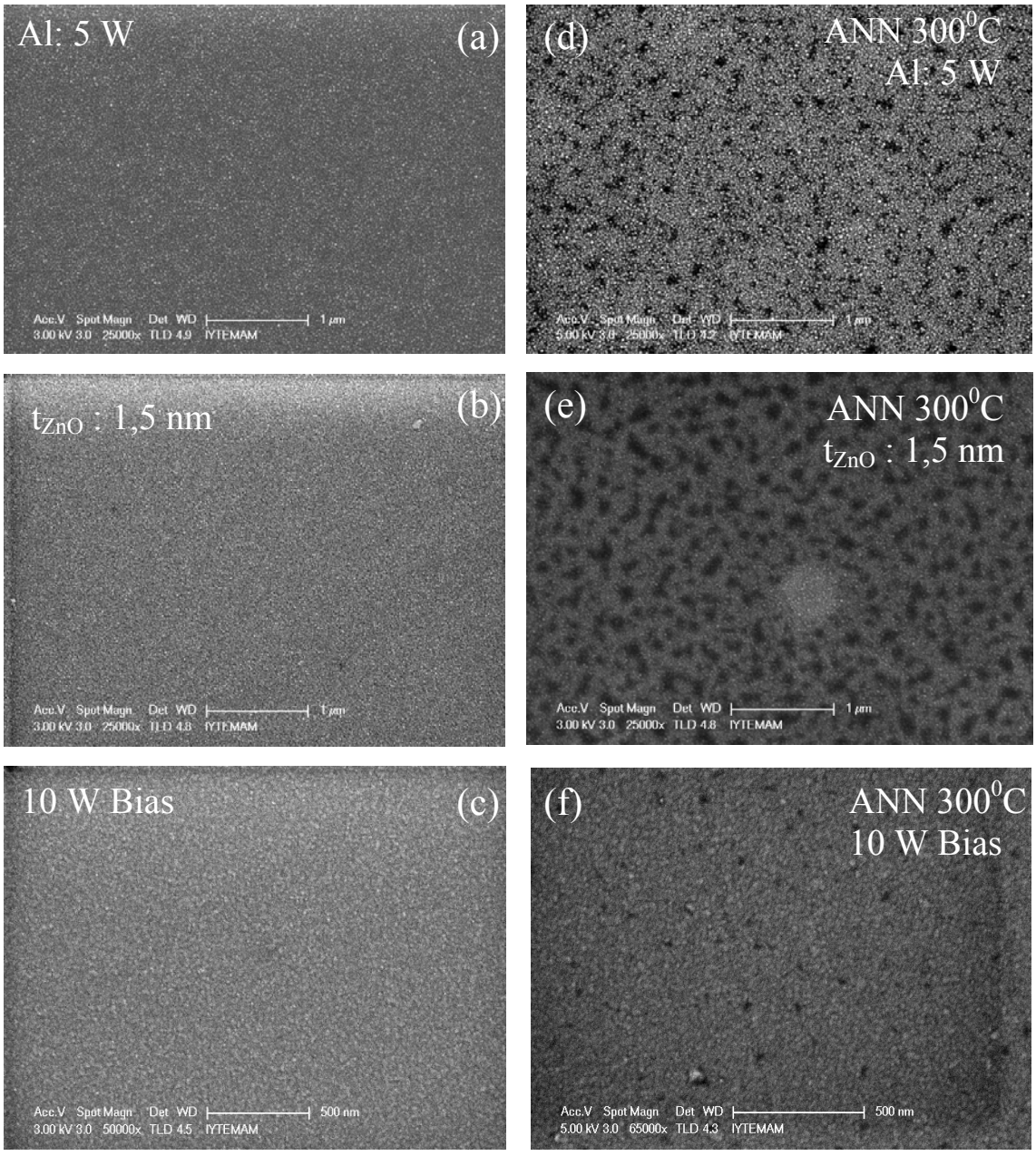

Figure 4.36. Comparison of (a,b,c) as grown and (d,e,f) annealed uniformly doped ZnO films. (lowest resistivity films of each set.) (a,d) uniformly doped (b,e) modulation doped, and (c,f) biased samples.

It was seen on the images that annealing caused a significant change on film surface. On the surface of annealed film, black dots and stains appeared. These stains were thought to be originated from dislocation of Al atoms with the effect of annealing. Al atoms are though to have gained thermal energy during annealing and this energy caused them coalescence together on particular sites of the film. The stains might be originated either from accumulated Al atoms forming Al clusters or vacancies left from removed Al clusters.

It was observed that on modulation doped samples, local strains were larger when compared to uniformly doped and biased sample. Indeed, on biased samples dots were much smaller compared to the other annealed samples, implying that annealing changed the surface of biased samples in the least significant way. (Therefore, SEM picture of biased sample was taken with 500 nm scale, whereas pictures of other samples were 1 μm.) This might be due to the fact that in biased samples, Al content was thought to be less than other films in the beginning.

4.5.3. Transmission Results

Transmission results showed that annealing did not cause significant change in transmittance, as can be seen on Figure 4.37. Similarly, band gaps did not change significantly with annealing for all sets.

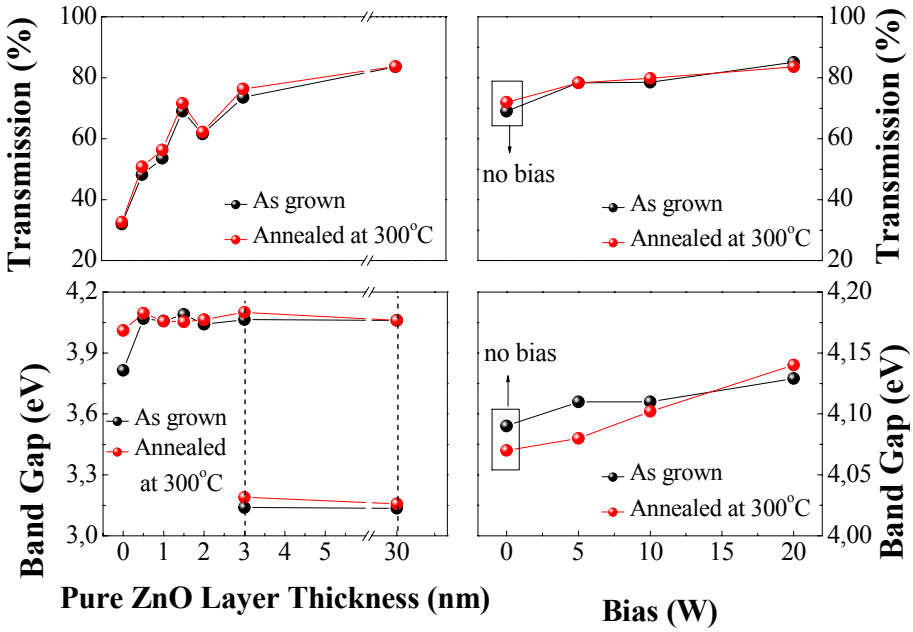

Figure 4.37. Average transmission and band gap values of annealed and non annealed samples (modulation doped and biased samples).

4.5.4. Resistivity

Figure 4.38 shows effect of annealing on resistivities of the samples. Resistivity of all the samples decreased to nearly half of the as grown value. According to XRD data, this drop could not be related to improvement of crystallinity. However, it is known that (Oh, et. al.) negatively charged oxygen ions act as trapping sites and form potential barriers. If oxygen was removed from the boundaries, carrier concentration and Hall mobility may have been increased, causing the decrease of resistivity by half. Resistivity of the lowest film (10 W substrate biased modulation doped film) dropped to 1.68×10^{-3} Ωcm with annealing.

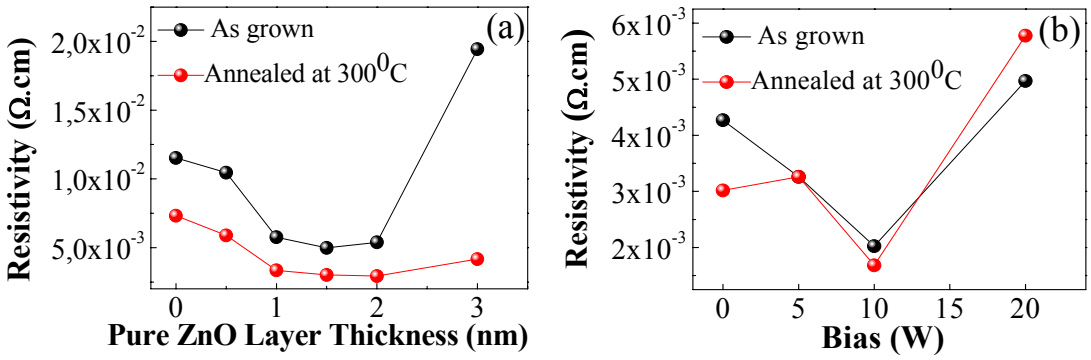

Figure 4.38. Resistivites of annealed and non annealed (a) modulation doped and (b) biased samples.

Decrease in resistivity might be reasoned to decrease of scatterings from impurities on particular sites of the film. SEM images showed that Al atoms might have gain thermal energy during annealing process and coalescence together. On the parts they left, Al content might have decreased leading to less scatterings on those regions. This might have led to increase in mobility and decrease in resistivity.

4.6. Summary

In summary, ZnO films are doped with Al. It was seen that lower concentrations showed lower resistivity and higher transmission values. Al content in the films were decreased in 3 processes. Every process was applied to the lowest resistivity sample of the previous process. The transmittance and resistivity results belonging to the best quality of each process are given in Figure 4.39.

Firstly, films were uniformly doped and content was lowered by decreasing deposition power of Al. These films showed rather high resistivity ($1.15x10^{-2}$ Ωcm) poor transmittance (32%). When the film with lowest resistivity was redeposited with modulation doping, resistivity of the sample decreased to $4.98x10^{-3}$ Ωcm and transmittance increased to 69%. Following this, modulation doped films with the lowest resistivity was deposited with various substrate biases. Substrate bias further improved electrical and optical properties of the film. Substrate biasing decreased the resistivity of the films to $2.03x10^{-3}$ Ωcm and transmittance increased to 79%.

Annealing films at 300°C in vacuum decreased their resistivities. Lowest resistivity (of the film 10 substrate biased modulation doped film) dropped to 1.68×10^{-3} Ωcm with annealing. Transmission of the same films became 80% as well.

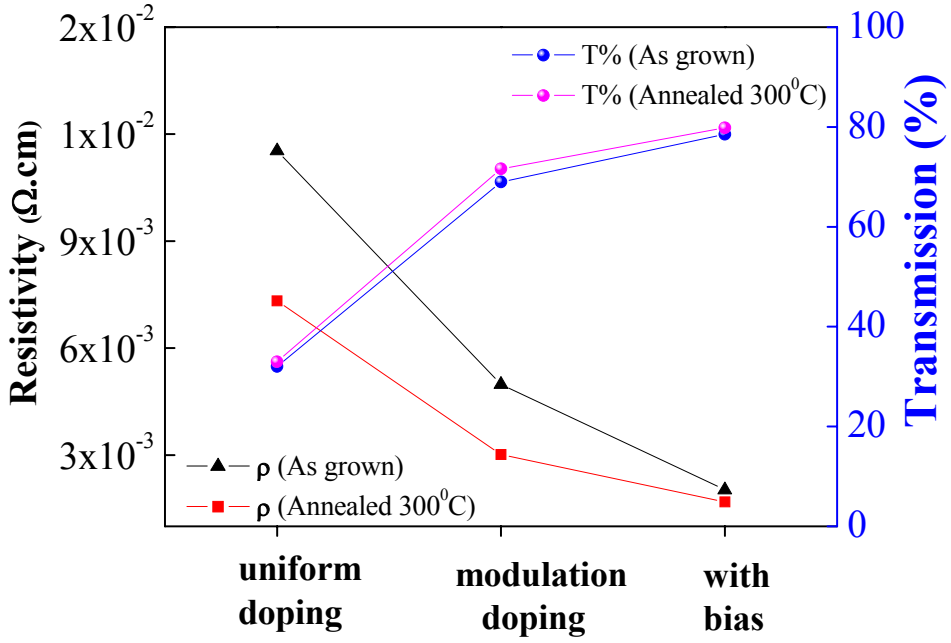

Figure 4.39. Resistivity and transmission values of lowest resistivity films of uniformly doped, modulation doped and substrate biased films.

CHAPTER 5

CONCLUSIONS

This thesis focused on growth, characterization and understanding physical properties of transparent and conducting Al doped ZnO thin films to be used especially as a front contact for solar cell devices.

In Chapter 1, some information about TCOs was given. TCO materials were compared and some applications of TCO materials were presented.

In Chapter 2, properties of ZnO were introduced. Detailed information about crystal structure, mechanical, electrical and optical properties of ZnO were given. Conduction mechanism and band structure of ZnO were explained. ZnO as compared to other TCOs and advantages and disadvantages of ZnO were summarized.

In Chapter 3 experimental details were presented. Magnetron sputtering technique was explained and fabrication process of thin films was described in detail. Films were characterized by AFM, surface profiler, XRD, SEM, UV-Vis spectrophotometer and four point electrical measurements.

In Chapter 4, results of structural, optical and electrical characterizations were discussed. Pure ZnO films with various thicknesses were characterized as well in order to be able to make a comparison between doped and undoped films.

Resistivity of pure ZnO films was very high to be measured with our instrument (>21.1 MΩsq). This indicated that intrinsic defects in ZnO were not enough to make the film conductor enough to be used as a transparent contact. Crossectional SEM picture proved that films were growing in columnar structure. XRD spectrums showed that ZnO films had polycrystalline structure. Films were highly textured and showed preferred orientation in (002) direction. Thicker films showed higher intensity in XRD spectrum indicating the increase in amount of crystallites in thicker films. However surface SEM pictures did not show a grainy structure. Pure films were highly transparent, but transmission values were decreasing with increasing thickness. Band gap of the films were found to be between 3.06 and 3.25 eV. Band gap of 30 nm thick (30 min deposited) ZnO film was 3.14 eV. Deposition thickness of ZnO was defined to be 30 nm (30 min) for the rest of the study.

In order to improve ZnO films conductance, 30 nm films were doped with Al by codeposition from ZnO and Al targets. 3 sets of experiment were performed, namely uniform doping, modulation doping and deposition with bias. Every set was aimed to further decrease the resistivity and increase transmittance of the best sample achieved in the previous set.

Firstly we doped films uniformly and decreased Al content by decreasing deposition power of Al from 20 W to 2.5 W. The lowest resistivity of 1.15×10^{-2} Ωcm with a poor transmittance of 32% were obtained with 5 W. XRD results showed that (002) peak vanished and a small peak in (101) direction showed up. This implied that introducing Al at these concentrations deteriorated crystal structure of the films, suggesting that Al did not replace Zn substitutionally and turned preferred orientation from (002) to (101). Low intensities implied that most of Al was located in interstitial sites. Also, when Al power was 20W, peaks belonging to metallic Zn in hexagonal structure occurred. This was explained by Al atoms taking O of ZnO in hexagonal lattice and being oxidized. Surface SEM pictures of Al doped films showed grainy structure, opposite to pure ZnO films. Films doped with power of 20 W had larger grains than those of films doped with 5 W. Based on XRD results, it was concluded that these grains were not oriented. This suggests that grains were formed by disordered Al clusters in the films. When deposition power was decreased to 2.5 W, a small peak in (002) direction reappeared. This was attributed to decrease in amount of Al. Resistivity results showed that when we introduced Al into the structure, conductivity improved substantially, however their transmittance decreased considerably. This was attributed to formation of impurity clusters owing to over doping. Free carriers were predicted to be scattered from these impurity centers leading to decrease in their mobility. In addition to scattering from impurity clusters, grain boundary scattering can be blamed for highly doped films due to their poor crystallinity as well.

In order to decrease doping concentration and increase mobility, we applied modulation doping, which can be summarized as deposition by thin layers of highly doped (doping layer) and undoped regions (transport layer).We changed the thickness of transport layer (pure ZnO) by timing, while fixing the doping layer thickness to ~1 nm (content of doped layers was fixed as well). XRD results showed that opposite to uniform doping, which degraded the crystal structure, modulation doping resulted in recrystallization in (002) direction. As pure ZnO layer thickness increased, orientation in (002) direction became stronger. In fact films with 3 nm stacks of pure ZnO showed

nearly the same crystal structure with pure ZnO film. Resistivity of modulation doped films was decreased to 4.98×10^{-3} Ωcm and transmission of the corresponding film reached to 69% (thickness of transport layers of the film was ~1.5 nm). Decrease of resistivity due to modulation doping might be attributed to improved crystal structure, leading to increase in mobility, which can be confirmed by XRD results. XRD results of modulation doped films showed that transport layers (pure ZnO) were polycrystalline. Therefore it can be concluded that carriers would suffer less from grain boundary scattering and impurity clustering scattering in transport layer, which would lead to increase in mobility and conductivity. When SEM picture of uniformly and modulation doped films (with lowest resistivities) were compared, it was seen that grains of modulation doped films were smaller. Increase of transmittance in these films may be attributed to decrease in Al content, leading to larger band gaps, therefore decreasing absorptions.

Lastly, we deposited this film by applying different bias powers to the substrate, resulting in additional Ar plasma during deposition. The process was a combination of sputtering and back sputtering. Crystal structure was expected to be improved as reported in literature, however according to XRD data, crystal structure of our samples degraded. Since surface of the film was being bombarded due to bias voltage, sticking of species onto the substrate may have been prevented, resulting in decrease of crystallinity. It was observed that preferred orientation tend to change from (002) to (101) plane. There was not a significant change in SEM pictures. When 20 W was applied, resistivity exceeded the resistivity of non biased sample. With this high bias power, sputtered species might be scattered before reaching the surface of the substrate, or even they reached, they might not be energetic enough to stick and migrate on the surface to form high quality film. These would lead to decrease in deposition rate of Al and Zn. If enough Al could not incorporate into the film, resistivity might have increased due to lack of donors. When bias power was decreased to 5W and 10W, resistivities of the samples decreased while transmittance of the samples increased. The lowest resistivity of 2.03×10^{-3} Ωcm was achieved with 10 W bias. Transmission of the corresponding film was 79%, including glass substrate. Improvement of conductance with substrate bias can not be explained with improvement of crystal structure unlike some work in literature. The reason of the improvement can be decrease of Al content in the film due to decrease in deposition rate as, still having sufficient amount. Transmission and band gap of the films increased with bias application. As mentioned

before, 10 W biased film had the lowest resistivity. Transmission and band gap of corresponding film was 78.5% and 4.11 eV respectively.

All samples were subjected to post deposition annealing. When samples were annealed at 300^{o}C degree in vacuum environment, it was observed that resistivity values were dropping to half of the initial value, whereas transmission values did not change significantly. Decrease in resistivity could not be related to improvement of crystal structure according to XRD data. The reason of decrease in resistivity was attributed to removal of O atoms from grain boundaries. If negatively charged oxygen ions were removed from grain boundaries, they would not form trapping sites and form potential barriers and this would lead to increase in mobility. Lowest resistivity (of the film 10 W substrate biased modulation doped film) dropped to 1.68×10^{-3} Ωcm with annealing. Transmission of the same films became 80% as well. Annealing was shown to be an effective and repeatable method to obtain more conducting films.

In summary, Al doping improved conductivity of ZnO films however decreased transmission considerably. Modulation doping and substrate bias decreased resistivity of films as well as increasing their transmission. Post deposition annealing decreased resistivity of films further, however transmittance of the films remained almost the same. Al doped ZnO films with the lowest resistivity of 1.68×10^{-3} Ωcm and with transmittance of 80% and band gap of 4.1 eV was fabricated by modulation doping accompanied with substrate bias of 10 W, followed by annealing at 300^{o}C in vacuum environment.

According to our results, modulation doping, deposition assisted with substrate bias and post deposition annealing were shown to be applicable methods to grow conductive and transparent thin films.

REFERENCES

Agura H., A. Suzuki, T. Matsushita, T. Aoki , M. Okuda. 2003. Low resistivity transparent conducting Al-doped ZnO films prepared by pulsed laser deposition. *Thin Solid Films* 445:263

Bai, S. N., T. Y. Tseng. 2009. Electrical and optical properties of ZnO:Al thin films grown by magnetron sputtering. *Journal of Materials Science: Materials in Electronics* 20: 253–256.

Bashar, S. A 1998. Study of Indium Tin Oxide (ITO) for Novel Optoelectronic Devices. *PhD diss*., University of London

Bates, C. H., W. B. White, R. Roy. 1962. New High-Pressure Polymorph of Zinc Oxide. *Science* 137:993.

Brooks, H. 1955. *Advances in Electronics and Electron Physics* 7: 85

Caihong, J., Y.Chen, G. Liu, X. Liu, S. Yang, Z. Wang. 2008. Growth of c-oriented ZnO films on (001) SrTiO3 substrates by MOCVD. *Journal of Crystal Growth* 311: 200–204

Chopra, K. L., S. Major, D. K. Pandya. 1983. Transparent conductors- A status review. *Thin Solid Films* 102: 1

Chung, Y. M., C. S. Moon, W. S. Jung, J. G. Han. 2006. The Low Temperature Process of Al doped ZnO films on glass and polymer using pulsed co-magnetron sputtering: H_2 Effect. *Thin Solid Films* 515: 567-570.

Cohen, D. J., S. A. Barnett. 2005. Predicted electrical properties of modulation-doped ZnO-based transparent conducting oxides. *Journal of Applied Physics* 98: 053705

Coleman, V.A, C. Jagadish. 2006. *Zinc Oxide-Bulk, Thin Films and Nanostructures.* Elsevier

Coleman, V.A. 2006. Processing and characterisation of ZnO for device applications. *PhD. diss,* The Australian National University.

Conwell, E., V.F. Weisskopf. 1950. Theory of Impurity Scattering in Semiconductors *Physical Review* 77:388

Dawar, A.L, J.C. Joshi. 1984. Semiconducting transparent thin films: their properties and applications. *Journal of Material Science* 19: 1

Dekkers J. M. 2007. Transparent conducting oxides on polymeric substrates. *PhD diss.*, University of Twente.

Dingle, R., H. L. Stromer, A. C. Gosard, W. Wiegman. 1978. Electron mobilities in modulation‐doped semiconductor heterojunction superlattices. *Applied Physics Letters* 33: 665.

Ellmer, K., G.Vollweiler. 2006. Electrical transport parameters of heavily-doped zinc oxide and zinc magnesium oxide single and multilayer films heteroepitaxially grown on oxide single crystals. *Thin Solid Films* 496: 104 – 111.

Ellmer, K., A. Klein, B. Rech. 2008. *Transparent Conductive Zinc Oxide Basics and Applications in Thin Film Solar Cells*. New York: Springer.

Ellmer, K. 2000. Magnetron sputtering of transparent conductive zinc oxide: relation between the sputtering parameters and the electronic properties. *Journal of Physics D: Applied Physics* 33: R17–R32.

Ellmer, K. 2001. Resistivity of polycrystalline zinc oxide films: current status and physical limit. *Journal of Physics D: Applied Physics* 34: 3097.

Erhart, P., K. Albe, A. Klein. 2006. First-principles study of intrinsic point defects in ZnO: Role of band structure, volume relaxation, and finite-size effects. *Physical Review B* 73: 205203.

Fragala, M. E., G. Malandrino, M. M. Giangregorio, M. Losurdo, G. Bruno, S. Lettieri, L. S. Amato, P. Maddalena. 2009. Structural, Optical, and Electrical Characterization of ZnO and Al-doped ZnO Thin Films Deposited by MOCVD. *Chemical Vapor Deposition* 15: 327:333.

Franken, R. H. J. 2006. Transparent conducting oxide contacts and textured metal back reflectors for thin film silicon solar cells. *PhD diss.,* Utrecht University.

Gordon, R.G. 2000. Criteria for choosing transparent conductors. *Material Research Society Bulletin* 25: 52. www.mrs.org/publications/bulletin (accessed March 2009).

Hao, X. T., L. W. Tan, K. S. Ong, F. Zhu. 2006. High-performance low-temperature transparent conducting aluminum-doped ZnO thin films and applications. *Journal of Crystal Growth* 287: 44–47.

Hartnagel, H. L, A. L. Dawar, A. K. Jain, C. Jagadish. 1995. *Semiconducting Transparent Thin Films.* Philadelphia, PA: Institute of Physics Publishing.

Halliburton, L. E., N. C. Giles, N. Y. Garces, M. Luo, C. Xu, L. Bai, L. Boatner. 2005. Production of native donors in ZnO by high temperature annealing in Zn vapor. *Applied Physics Letters* 87:172108/1-172108/3.

Jenkins, D. F. L., M. J. Cunningham, G. Velu, D. Remiers. 1997. The use of sputtered ZnO piezoelectric thin films as broad-band microactuators. *Sensors Actuators* A 63:135.

Jeong, W. J., G. C. Park. 2002. Electrical and optical properties of ZnO thin films as a function of deposition parameters. *Solar Energy Materials & Solar Cells* 65: 37-45

Joshua, J. R., Wolden C. A. 2003. High mobility oxides: Engineered structures to overcome intrinsic performance limitations of transparent conducting oxides *Applied Physics Letters* 83: 3933-3935.

Kerkache, L., A. Layadi, E. Dogheche, D. Remiens. 2006. Physical properties of RF sputtered ITO thin films and annealing Effect. *Applied Physics* 39:184 -189.

Kittel C. 2005. *Introduction to Solid State Physics*, eds 8. California: Wiley.

Lany, S., A. Zunger. 2005. Anion vacancies as a source of persistent photoconductivity in II-VI and chalcopyrite semiconductors. *Physical Review B* 72:03215/1-03215/13

Lee, J. H., J. T. Song. 2008. Dependence of electrical and optical properties on the bias voltage for ZnO:Al films deposited by r.f. magnetron sputtering. *Thin Solid Films* 516: 1377-1381.

Lide, D. R. 1992. *Handbook of Chemistry and Physics*, 73rd Edition, New York: CRC Press.

Markets for Zinc Oxide in Electronics. 2008. *Nano-053* http://nanomarkets.net/market_reports/report/ (accessed November 2009)

Minami, T. 2005. Transparent conducting oxide semiconductors for transparent electrodes. *Semiconductor Science and Technology* 20: S35–S44.

Minami, T., H. Nanto and S. Takata. 1984. Calculation of Bond Length in $Ga_{1-x}In_xAs$ Ternary Semiconductors. *Japanese Journal of Applied Physics* 23: L280.

Minami, T., H. Sato, S. Takata, N. Ogawa, T. Mouri. 1992. Large-Area Milky Transparent Conducting Al-Doped ZnO Films Prepared by Magnetron Sputtering. *Japanese Journal of Applied Physics* 31: L1106.

Moon, C. S., Chung Y. M., Jung W.S., Han J.G. 2007. The low temperature process design for Al doped ZnO film synthesis on polymer. *Surface and Coatings Technology* 201: 5035-5038.

Morkoc, H., U. Ozgur. 2009. *Zinc Oxide Fundementals, Materials and Device Technology. Weinheim: Wiley-VHC*

Nakazawa, H., Y. Ito, E. Matsumato, K. Adachi, N. Aoki, Y. Ochai. 2006. The electronic properties of amorphous and crystallized In_2O_3 films. *Journal of Applied Physics* 100:093706/1-09370/8

Oh, B. Y., M. C. Jeong, D. S. Kim, W. Lee, J. M. Myoung. 2005. Post-annealing of Al-doped ZnO films in hydrogen atmosphere. *Journal of Crystal Growyh* 281: 475–480.

Oksuzoglu, R. M., O. Gonenc, N. C.Aslandere, H. Cinar, M. Yildirim. Thin Film Process and characterization laboratory I and II Script for theoretical and experimental preparation.

Ozgur, U. 2005. A comprehensive review of ZnO materials and devices. *Journal of Applied Physics* 98: 04130.

Pankove, J. 1975. *Optical Processes in Semiconductors*. New York:Dover

Rauf, I. A. 1993. Low resistivity and high mobility tin-doped indium oxide films *Materials Letters* 18: 123-127

Robbins, J. J., C. A. Wolden. 2003. High mobility oxides: Engineered Structures to overcome intrinsic performance limitations of transparent conducting oxides. *Applied Physics Letters* 83: 3933-3935.

Sato, H., T. Minami, S .Takata, T. Miyata and M. Ishii. 1993. Fabrication of high-Tc superconductors using ozone-assisted molecular beam epitaxy. *Thin Solid Films* 236:14

Satoh, I., T. Kobayashi, K. Katayma, T. Okada, T. Itoh. 2004. Magneto-photoluminescence of novel magnetic semiconductor $Zn_{1-x}Cr_xO$ grown by PLD method. *Applied Physics A* 79:1445

Schropp, R. E., I. C. E. Matovich, P. K. Bhat, A. Madan. 1988. Transparent and conductive thin films of ZnO for photovoltaic applications prepared by RF magnetron sputtering. IEEE 273-276.
http://sciencestage.com/d/3579097.html/ (accessed April, 2010)

Singh, A. V., R. M. Mehra. 2001. Highly conductive and transparent aluminum-doped zinc oxide thin films prepared by pulsed laser deposition in oxygen ambient. *Journal of Applied Physics* 90: 5661-5665.

Suzuki, A. 2009. Transparent Conductive Zinc Oxide Film New Light for Indium-free Solar Cells. *ULVAC Technologies Magazine* 56:18-21.

Suzuki A, T. Matsushita, N. Wada, Y. Sakamoto and M. Okuda. 1996. Transparent Conducting Al-Doped ZnO Thin Films Prepared by Pulsed Laser Deposition. *Japanese Journal of Applied Physics* 35: L56

Tel Aviv University. Review of TCO Thin Films.
http://www.eng.tau.ac.il/ (accessed October 2009)

Van de Walle, C.G. 2000. Hydrogen as a cause of doping in zinc oxide. *Physical Review Letters* 85:1012-1015

Weiher, R. L., R. P. Ley. 1966. Optical Properties of Indium Oxide. *Journal of Applied Physics* 37:299

Wager, J. F., D. A. Keszler, R.E. Presley. 2008. *Transparent Electronics*. New York: Springer

Webb, J. B., D. F. Williams, M. Buchanan. 1981. Transparent and highly conductive films of ZnO prepared by rf reactive magnetron sputtering. *Applied Physics Letters* 39: 640.

Wit, J. H. W. 1977. Electron concentration and mobility in In_2O_3. *Journal of Physics and Chemistry of Solids* 38:819-824.